JAYCOR

300 Unicorn Park Drive
Woburn, Massachusetts 01801

A REVIEW OF AN ATTEMPT TO CREATE SHATTER CONES WITH MAGNETIC FLYER PLATE TECHNOLOGY

JAYCOR Project #2185

Final Report On NASA

Contract No. NASW-3328

J206-81-005-FR

April 8, 1981

Submitted to:

NASA Headquarters
Washington, DC 20546

SECURITY CLASSIFICATION OF THIS PAGE (When Data Entered)

REPORT DOCUMENTATION PAGE		READ INSTRUCTIONS BEFORE COMPLETING FORM
1. REPORT NUMBER J206-81-005-FR	2. GOVT ACCESSION NO.	3. RECIPIENT'S CATALOG NUMBER
4. TITLE (and Subtitle) A Review Of An Attempt To Create Shatter Cones With Magnetic Flyer Plate Technology		5. TYPE OF REPORT & PERIOD COVERED Final Report 11/28/79 - 11/28/80 6. PERFORMING ORG. REPORT NUMBER J206-81-005-FR
7. AUTHOR(s) Dr. Harold J. Linnerud		8. CONTRACT OR GRANT NUMBER(s) NASW-3328
9. PERFORMING ORGANIZATION NAME AND ADDRESS JAYCOR 300 Unicorn Park Drive Woburn, Massachusetts 01801		10. PROGRAM ELEMENT, PROJECT, TASK AREA & WORK UNIT NUMBERS
11. CONTROLLING OFFICE NAME AND ADDRESS NASA Headquarters Washington, DC 20546 Attn: Dr. William Quaide Code SL-4		12. REPORT DATE 8 April 1981 13. NUMBER OF PAGES 73
14. MONITORING AGENCY NAME & ADDRESS(if different from Controlling Office) Same as block 11		15. SECURITY CLASS. (of this report) UNCLASSIFIED 15a. DECLASSIFICATION/DOWNGRADING SCHEDULE

16. DISTRIBUTION STATEMENT (of this Report)

NASA Scientific and Technical Information Facility (1 Reproducible + 2 copies)
P.O. Box 8757, Baltimore/Washington International Airport, Baltimore,MD 21240

NASA Headquarters (1 Reproducible + 10 copies)
Washington, DC 20546 - Att: Dr.William Quaide Code SL-4

(continued)

17. DISTRIBUTION STATEMENT (of the abstract entered in Block 20, if different from Report)

18. SUPPLEMENTARY NOTES

19. KEY WORDS (Continue on reverse side if necessary and identify by block number)

Shatter Cones
Magnetic Flyer Plate
Shock Wave

20. ABSTRACT (Continue on reverse side if necessary and identify by block number)

An experiment using magnetic flyer plate technology to generate high amplitude shock waves in test materials is described. Program goal was to demonstrate the feasibility of creating shatter cones in a controlled laboratory environment. Although considerable sample shear and break up was observed, to date no shatter cones have been found in the tested samples.

DD FORM 1 JAN 73 1473 EDITION OF 1 NOV 65 IS OBSOLETE
S/N 0102-LF-014-6601

UNCLASSIFIED
SECURITY CLASSIFICATION OF THIS PAGE (When Data Entered)

Continued From Block 16 "Distribution Statement (of this Report)"

NASA Headquarters (1 Copy of the Letter of Transmittal of the Final Report)
Washington, DC 20546
Attn: Contract Administration Branch
Code HWC-2

TABLE OF CONTENTS

I. INTRODUCTION

Shatter cones are a curious mode of rock fracture which appear to be produced by intense shock. They have been observed in, or near, natural crater sites [1-6], after certain high-explosive and nuclear detonations[7-9], and in selected hyper-velocity impact (HVI) experiments[10,11]. An excellent review of their characteristics and of their occurrence has been presented by Dietz[12]. Currently, their presence in natural craters is being used to ascribe crater origin to impact by an extra-terrestrial body as opposed to any endogenetic mechanism.

Shatter cones which have been produced either by explosive tests or by HVI experiments generally are oriented with their apices pointed toward the source of the disturbance which created them. In natural craters (once gross upheavals have been corrected for) the same trend is observed where cone apices are oriented upward and toward the crater center. Natural shatter cones have been observed as large as 15 m (the Kentland structure[1]), high-explosive (HE) or nuclear testing has produced them as large as 1 meter[7] and HVI formed shatter cones have generally been limited to several mm in length[10]. Recent work has reported the observance of melt spherules on the surface of Vredefort shatter cones[13] to show local melting and then considerable dilation to preserve the spherules. Roddy[7] has reported the creation of shatter cones in a series of Department of Defense (DoD) high explosive tests and has compared the geometry of occurrence with cratering calculations to bound formation shock intensity at 20 to 60 kilobars (kB). Other observers have surmised required shock intensities as high as 100 kB[14].

It would appear that shatter cones could be used as a positive indicator of origin for certain craters, but also that they might be useful in estimating shock amplitudes (and therefore formation energy). We know that shatter cones can be formed by shock waves generated during explosive tests and hypervelocity impacts, but we do not know the mechanics of shatter cone formation, the formational pressure range, and what can be deduced about the overall impact process from the presence of shatter cones in various rock types. Theoretical studies of shatter cone formation are limited[15-17], but give some clues as to what may be the key factors to consider in a definitive investigation.

Described in this report is an attempt to create shattercones in a controlled laboratory environment. More importantly, the technique used to load selected test samples (magnetic flyer plates) was thought to be capable of creating shattercones considerably larger than those created previously with hyper-velocity impact (HVI) experiments.

The remainder of this report presents more background on shattercones, describes the laboratory technique used in the attempt to generate them and discusses results obtained.

II. BACKGROUND

Shatter cones, as "Strahlenkalk", were first reported in 1905 by Branca and Fraas[18]. They found shatter cones in the Steinheim Basin of South Germany and ascribed their source to a pressure phenomenon. Extensive reviews of shatter cones have been published by Dietz[2,3,12] who diretly associates their natural occurrence with impacts from extraterrestrial bodies

The details of his theory can be found in the above references and will only be summarized here:

1. Natural shatter cones are only found in or near some, but not all, crater-like structures.
2. The mode of failure which creates shatter cones does not take place along pre-existing lines of natural weakness. This might imply that they were formed by an intense and almost instantaneous force which over-rode expected splintering geometries.
3. Man-made shatter cones have only been produced by HVI and high-explosive or nuclear detonations where high-velocities or shock intensities have exceeded certain thresholds
4. Tectonic, magnetic or volcanic forces do not reach the thresholds felt necessary for shatter cone formation.
5. Natural shatter cones are most often in direct proximity with other shocked or metamorphed materials that can similarly be created in high-intensity shock events.

Roddy's recent review[7] generally supports and amplifies these same con-

clusions. Some, or all, of the above are generally invoked to conclude that the presence of shatter cones in crater-like structures such as Steinheim, Reis, Wells Creek, etc. implies that their source was an impact event with an extraterrestrial body.

Most of our current knowledge on shatter cones is very qualitative. For natural shatter cones, essentially nothing is known about the physical properties and/or phenomenology which governed their formation. Those created in explosive testing were only observed as effects secondary to the prime goals of the tests and hence instrumentation appropriate to characterizing conditions during their formation was not used. Roddy has recently correlated cratering calculations with the observed location of shatter cones for several DoD HE tests[7] to estimate a formational pressure range of 40 ± 20 Kb for crystalline rock. In HVI tests, impact conditions can be well-defined, but there are large uncertainties in converting these conditions to shock parameters and the very scale of the shatter cones formed[10,11] makes accurate measurement of these same parameters difficult. Although a matter of some conjecture the actual physical mechanism (and the governing shock/material properties) which creates shatter cones is still unproven.

III. EXPERIMENTAL APPROACH

Experimental Program

As mentioned previously, shatter cones have been observed in presumed impact craters, in certain explosive events and in HVI testing. It is obvious from all of these sources that shatter cone formation is in some way related to the energy which these events deposit in the earth, or test materials, and it is presumed that there is a direct correlation with the intense shock waves which these events create. In all of these the shocks created are divergent, and in the case of large cratering events would even tend to locally approach planar behavior (relative to the size of the cones).

Although HVI testing can produce shatter cones, they are so small that they prevent efficient diagnostic monitoring and also inhibit extrapolation to the large-scale events of interest. Because of the techniques used in driving the test projectile to impact, HVI technology is limited in scope and cannot easily be scaled up to provide larger test events and therefore larger shatter cones.

One can consider the use of HE in generating the desired shock wave, but this implies two alternative approaches, neither of which is particularly desirable. Testing at levels over a certain size almost necessitates a fully developed field effort with the implied pre-event site characterization and instrumentation to permit valid diagnostics. The costs for such efforts are prohibitive and results can be very difficult to interpret.

The HE effort could be scaled-down to permit laboratory usage in testing selected samples of man-made and geologic material. Unfortunately, the desired shock planarity and intensity for properly scaled laboratory

events almost necessitates the use of light-initiated sheet explosives. Although within the state-of-the-art and feasible, the use of such explosives is extremely hazardous and toxic and will produce more safety and environmental problems than are warranted or necessary

In a careful review of tools and techniques which can be used to generate shocks of the amplitude felt necessary for shatter cone formation, magnetic flyer plate technology was identified as being particularly useful in this application. The technology was developed to meet DoD needs (see below), is controllable, reproducible, clean and non-toxic. It is this approach which was employed to simulate the desired shock amplitudes

Magnetic Flyer Plate Technology

Magnetic flyer plate technology was developed by the DoD to simulate the effects of short duration high level x-ray exposure. X-rays have an extremely short range in most materials and a surface exposed to such a flux is immediately dosed to a high energy level. This energy can then generate a propagating shock.

To simulate this intense shock, the DoD developed magnetic flyer plate technology to where it is now routinely used in a controlled laboratory environment. To create the desired shock, a test target is impacted by a thin metallic sheet (the flyer) which is physically separated from the target by a small air gap. The flyer is backed by a dielectric and a load block and to initiate an impact event the flyer and load block are shorted across a capacitor bank system which has previously been charged to a known voltage level. The dumped electrical energy is converted into flyer kinetic energy by ExB forces, and a very real upper limit on impact

energy is defined by vaporization of the flyer material. Delivered shock amplitude may be varied by adjusting some, or all, of the following parameters: driving voltage, total energy, flyer material and flyer thickness.

The magnetic flyer plate system used in this experimental program can dump in excess of 300 kilojoules of electrical energy into impact areas as large as one square foot at shock levels as high as 50 to 60 kilobars. It was felt that these amplitudes should be large enough to effectively cover most geologies and events of interest.[7] The test configuration used for the experimental effort is outlined in Figure 1. Note that firmly embedding the test sample in a medium of matching shock propagation velocity is necessary to assure smooth passage of the shock wave out of the test sample and to prevent reflected shocks from complicating both calculational and experimental interpretation of results.

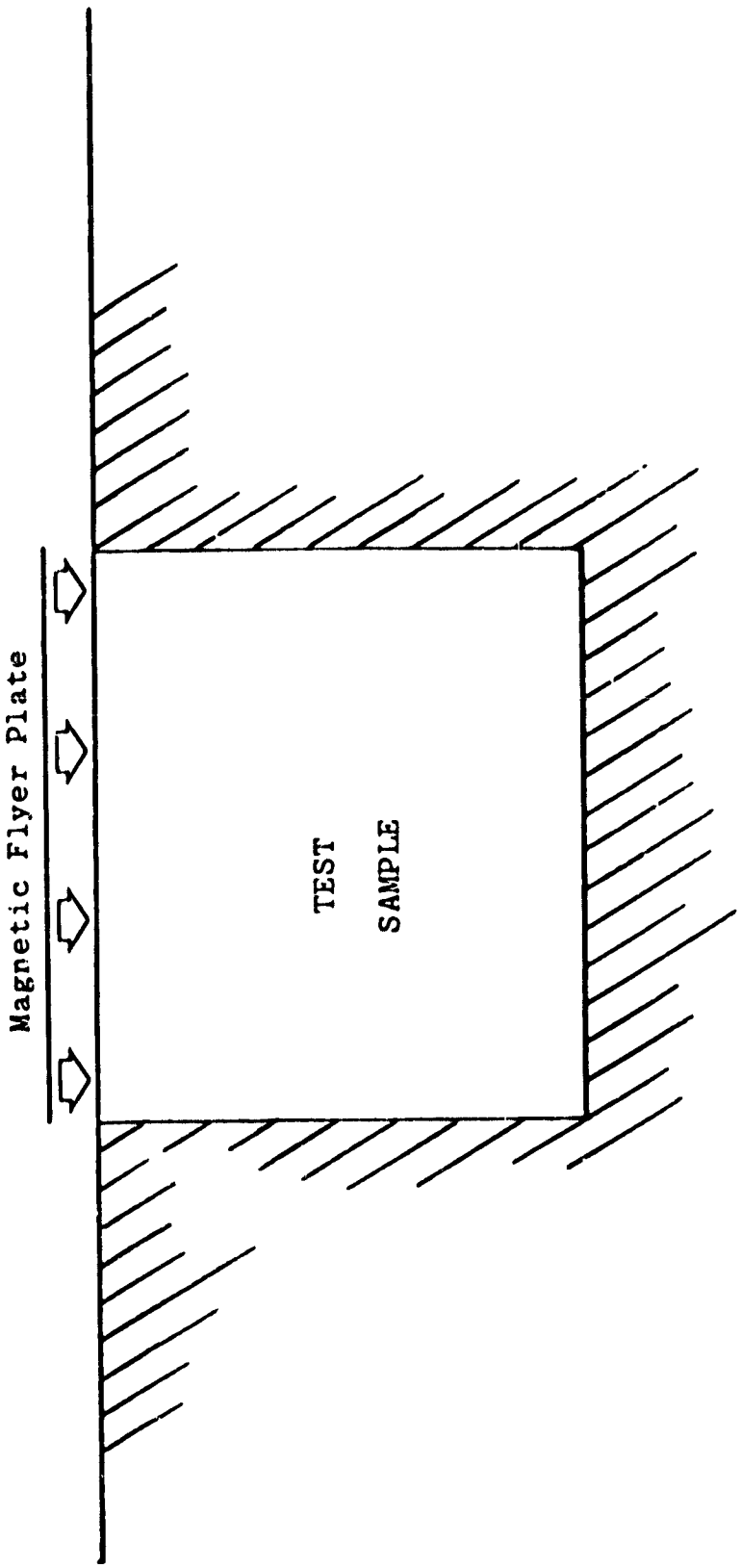

Figure 1 Impact Configuration for Shattercone Experiments

IV. RESULTS

The experimental work on this program was conducted over a two week period in August of 1980 at the Science Applications Inc. Laboratory in Las Vegas, Nevada. Their flyer plate facility, plus the results of the tests performed, are described in Appendix A.

Prior to conducting these tests, Drs. Roddy and Curran worked with JAYCOR to define some of the tests to be conducted and the test conditions. Dr. Curran summarized his input in the letter which is attached as Appendix B.

Three types of samples were tested in this program: plexiglass blocks obtained from DuPont, grout (cement) blocks cast by JAYCOR and limestone samples secured by Dr. Roddy. Each of these samples was embedded in compacted sand to provide impedance matching and delivered loads ranged from 10 kB to 80 kB measured by mounted manganin gauges. Table I, taken from Appendix A, summarizes the test program.

Of the three types of samples tested, the limestone proved to be the most valuable. The plexiglass samples tended to exhibit large shear surfaces with a considerable amount of rear surface spall. The grout samples were made with an aggregate which too proved to be too coarse and the air bubble inclusion level was too high. The limestone samples provided by Dr. Roddy were extremely uniform and fine-grained and would have shown the sought-for features quite readily.

All samples were embedded in the compacted sand and impacted with aluminum flyer plates which ranged from 5 to 10 cm wide. These flyer plates delivered a planar shock wave from 10 to 80 kb strong.

TABLE 1

SUMMARY OF TEST DATA

SAI Shot	Sample/(No.)	Flyer Width (cm)*	Bank Volts (kV)	Current Monitor (V)	Pressure Est. (GPa)**	Pressure Meas. (GPa)**	Gage Depth (
34	MM/W (1)	5.08	25.0	9.55	6.5	6.5	- 2
35	SM/W (2)	5.08	25.0	7.64	5.2	4.3	- 2
36	MM/W (3)	5.08	25.0	6.14	4.2	---	---
37	MM/O (4)	5.08	25.0	7.44	< 1.0 (1)	---	---
38	Plexiglass (5)	5.08	25.0	11.00 est.	7.5	6.4	- 2
39	SM/W (6)	5.08	25.0	12.91	8.8	8.2	- 2
40	Limestone (7) Fine Grain	5.08	25.0	10.78	7.3	---	---
41	Plexiglass (8)	5.08	25.0	8.49	5.7	---	---
42	Limestone (9) Med. Grain	6.35	25.0	5.81	1.1	---	---
43	Limestone (10) Point Source	5.08	25.0	0	0 (1)	---	---
44	Rerun Shot 43	5.08	25.2	5.47	3.7	---	---
45	Limestone (13)	7.62	25.1	9.02	2.7	---	---
46	Limestone (14)	10.16	25.0	11.40	1.9	---	---
47	Limestone (11) (constrained)	5.08	25.0	4.95	3.4	1.8	- 4
48	Limestone (15)	7.62	25.0	6.30	1.9	---	---
49	Limestone (12)	7.62	24.9	6.33	1.9	2.1 --- (2)	3 38
50	Limestone (16)	6.35	25.0	4.30	1.9	0.52 0.09	8 37

* Flyer Density = 1.37 gm/cm^2
** 1GPa = 10kB
(1) Header Plate Breakdown
(2) No Record For Second Gage - Scope Did Not Trigger

Three of the samples were handled slightly differently. On one sample (#10) an attempt was made to generate a point source shock wave. The sample was covered with a sheet of 6.35 mm (0.25 inch) thick teflon which had a 12.7 mm (0.5 inch) diameter aluminum disc inserted in the teflon near the sample center. The teflon was intended to severely attenuate the delivered shock while the aluminum disc would directly couple the shock to the sample. This arrangement appeared to work quite well as an impression of the disc was found on the sample and the teflon was severely damaged with considerable blackening along the edge of the impact zone due to joule heating.

Another sample (#11) was constrained in attempt to minimize the fracturing seen on earlier tests and to more nearly approximate conditions found in the earth. Sheet aluminum stock (0.25 inch) was epoxy-bonded around the sample sides and these plates were then tension banded to generate a static pressure. The technique proved moderately successful and did indeed limit the observed sample shearing.

The final test sample (#16) was instrumented with two pressure gauges and several time-of-arrival guages. These gauges were used to measure the shock propagation velocity and yielded a value of approximately 2.5 km/sec. -- a not unreasonable number. Note also that the pressure gauge measurements show an attenuation from 0.52 GPa to 0.09 in just under 30 mm. This is a rapid attenuation rate but it is based upon only two measurements.

After all samples had been impacted, Drs. Roddy and Linnerud examined the samples in the SAI laboratory but could find no indication that shatter cones had indeed been formed. There was considerable evivdence

that all samples had undergone extremely high rates of shear and large numbers of sheared surfaces with suspicious "flutings" were recovered in most of the limestone samples. No similar evidence was found in the grout or plexiglass samples.

All samples have been taken by Dr. Roddy to the U.S.G.S. laboratory in Flagstaff, Arizona where he is continuing to examine them for evidence of shatter cone formation. It is not known whether his search will be successful, but it would appear that we have been unable to generate shatter cones in the manner desired.

V. REFERENCES

1. Dietz, R.S. (1947), Meteorite Impact Suggested by Orientation of Shatter Cones at the Kentland, Indiana Disturbance, Science, 105, p. 42-43.

2. _____ (1960), Meteorite Impact Suggested by Shatter Cones in Rock, Science, 131, p. 1781-1784.

3. _____ (1966), Shatter Cones and Astroblemes, Proc. Oregon Lunar Geological Field Conference, Bend, Oregon.

4. Hargraves, R.B. (1961), Shatter Cones in Rocks of Vredefort Ring, Geol. Soc. S. Africa Trans., 64, p. 147-153.

5. Howard, K. and Offield, T. (1968), Shatter Cones at Sierra Madera, Texas, Science, 162, p. 261-265.

6. Manton, W.I. (1965), The Orientation and Origin of Shatter Cones in the Vredefort Ring, Ann. N.Y., Acad. Sci., 123, p. 1017-1049.

7. Roddy, D.J. and Davis, L.K., Shatter Cones Formed in Large Scale Experimental Explosion Craters, Proc. of Symp. on Planetary Cratering Mechanics, to be published in The Moon.

8. Burch, T.E. and Quaide, W.L. (1968), Shatter Cones in the Danny Boy Nuclear Crater, in Shock Metamorphism of Natural Materials (editors: B.M. French and A.M. Short).

9. Roddy, D.J., and Davis, L.K. (1969), Shatter COnes at TNT Explosion Craters, Trans. AGU, 50, p. 220.

10. Schneider, E., and Wagner, G.A. (1976), Shatter Cones Produced Experimentally by Impact in Limestone Targets, Earth and Planetary Sci. Letters, 32, p. 40-44.

11. Shoemaker, E.M., et al. (1961), Shatter Cones Formed by High Speed Impact in Dolomite, U.S. Geol. Survey Prof. Paper 424-D, p. 365-368.

12. Dietz, R.S. (1963), Astroblemes: Ancient Meteorite-Impact Structures on the Earth, In The Solar System, V. 4, The Moon, Meteorites, and Comets, B.M. Middlehurst and G.P. Kuiper, eds., p. 285-300.

13. Gay, N.C. (1976), Spherules on Shatter Cone Surfaces From the Vredefort Structure, South Africa, Science, 194, p. 724-725.

14. Milton, D.J. (1976), Personal Communication.

15. Gash, P.J. Syme (1971), Dynamic Mechanism for the Formation of Shatter Cones, Natural Physical Science, 230, p. 32-35

16. Johnson, G.P., and Talbot, R.J. (1964), A Theoretical Study of the Shock Wave Origin of Shatter Cones, M.S. Thesis, Air Force Institute of Technology, Wright-Patterson AFB, Ohio, 92 p.

17. Curran, D.G., A Theoretical Model for Shatter Cone Formation, Poulter Laboratory Technical Report, Stanford Research Institute, July 1977.

18. Branca, W., and Fraas, E. (1905) Das Kryptovulkanitche Becken von Steinheim, Akad. Wiss. Bertin, Phys.-Math. Kl, Abh.1, 64 p.

APPENDIX A

MAGNETIC FLYER PLATE IMPACT TESTS ON CANDIDATE SHATTER CONE MATERIALS

WORK PERFORMED UNDER
JAYCOR PURCHASE ORDER 6729
NASA PRIME CONTRACT S-70206-B

science applications, inc.
3351 so. highland dr., suite 206
las vegas, nevada 89109

TABLE OF CONTENTS

TABLES

ILLUSTRATIONS

USE OF THE INTERNATIONAL SYSTEM OF UNITS (SI)

In this report, SI units will be used. Customary units may also be used for clarity. In those cases, SI units will be used first followed by customary units in parentheses.

1.0 INTRODUCTION

A series of tests have been conducted to investigate the feasibility of generating shatter cone rock fracture formations under laboratory conditions. Shatter cone formations have been found in natural crater sites, high explosives detonation sites and several hyper-velocity impact experiments. The presence of such formations in craters is believed to have been caused by pressures generated during impact by an extra-terrestrial body and the resultant crater formation. If shatter cones can be formed under laboratory conditions; then we may infer the origin of certain craters, the shock amplitudes during formation and possibly formation energy.

This report discusses laboratory tests that were conducted at the SAI Las Vegas Magnetic Flyer Plate Facility under contract to JAYCOR. Test samples were provided by Linnerude[1] and Roddy[2] who participated in the laboratory testing. This report discusses the laboratory setup, test procedures and data that were recorded. A detailed description of the test facility is included in Appendix A. Analysis of the recorded pressure and time of arrival data are presented. Analysis of the resultant rock fractures will be reported by Linnerude and Roddy in separate documentation.

During this program 16 samples were impacted at peak pressures ranging from 1GPa (10kB) to 8GPa (80kB). A summary of test data are listed in Table 1.1. Prior to impacting actual samples, SAI conducted a series of tests to characterize flyer plate performance and develop gage techniques to record the dynamic pressure delivered to the rock samples. For these tests, thin foil manganin gages were packaged to respond to the samples near surface shock pressure. The gage was designed to minimize magnetic noise coupling due to high currents flowing in the flyer plate (10^5 amperes).

---

(1) Dr. Harold Linnerude is with JAYCOR and was the principle investigator for this program.

(2) Dr. David Roddy is with the U. S. Geological Survey.

TABLE 1.1

SUMMARY OF TEST DATA

SAI Shot	Sample/(No.)	Flyer Width (cm)*	Bank Volts (kV)	Current Monitor (V)	Pressure Est. (GPa)**	Pressure Meas. (GPa)**	Gage Depth (m
34	MM/W (1)	5.08	25.0	9.55	6.5	6.5	- 2
35	SM/W (2)	5.08	25.0	7.64	5.2	4.3	- 2
36	MM/W (3)	5.08	25.0	6.14	4.2	---	---
37	MM/O (4)	5.08	25.0	7.44	< 1.0 (1)	---	---
38	Plexiglass (5)	5.08	25.0	11.00 est.	7.5	6.4	- 2
39	SM/W (6)	5.08	25.0	12.91	8.8	8.2	- 2
40	Limestone Fine Grain (7)	5.08	25.0	10.78	7.3	---	---
41	Plexiglass (8)	5.08	25.0	8.49	5.7	---	---
42	Limestone Med. Grain (9)	6.35	25.0	5.81	1.1	---	---
43	Limestone Point Source (10)	5.08	25.0	0	0 (1)	---	---
44	Rerun Shot 43	5.08	25.2	5.47	3.7	---	---
45	Limestone (13)	7.62	25.1	9.02	2.7	---	---
46	Limestone (14)	10.16	25.0	11.40	1.9	---	---
47	Limestone (11) (constrained)	5.08	25.0	4.95	3.4	1.8	- 4
48	Limestone (15)	7.62	25.0	6.30	1.9	---	---
49	Limestone (12)	7.62	24.9	6.33	1.9	2.1 --- (2)	3 38
50	Limestone (16)	6.35	25.0	4.30	1.9	0.52 0.09	8 37

* Flyer Density = 1.37 gm/cm^2
** 1GPa = 10kB
(1) Header Plate Breakdown
(2) No Record For Second Gage - Scope Did Not Trigger

2.0 PRESTEST CHARACTERIZATION

A series of 20 shots were conducted to characterize the flyer plates for use in the shatter cone experiment. The purpose was to characterize the impact pressure as a function of flyer plate width, density and capacitor bank voltage. In addition, a gage technique was developed to measure the impact pressure.

An aluminum flyer was selected to match the rock samples that were to be impacted in the test program. The rock composition was assumed to be SiO_2 which has a density of $2.6gm/cm^3$ as compared to an aluminum density of $2.7gm/cm^3$. As such, we would expect about 90 percent on the flyer momentum density to be transferred to the target on impact. During the pretest characterization series we used an aluminum target. Thus we would expect the energy transfer on impact to approach 100 percent. In reality, the impact transfer is modified slightly by air cushioning. This effect is dependent upon the flyer velocity and the standoff distance between the flyer and the target. Another effect to consider is that the aluminum density goes to $2.37gm/cm^2$ at its melting point. As a result, the flyer density may be reduced up to ten percent if it is made too small and joule heating is allowed to occur.

The flyer plate setup is shown in Figure 2.1. A standard target size was used for all tests. Manganin piezoresistive gages were bonded to each target and the gage output was measured during impact. In some tests, the gages were imbedded into the target by milling a channel into the aluminum. The gage was then bonded and the channel was filled with a matching piece of aluminum that was also bonded to the gage.

On many tests the gage leads were severed on impact. This was caused by the edge of the flyer which curls and creates a shear wave. To counter this problem, the gage channel was

deepened as it exited the target. This technique was successful. Several pressure records are shown in Figure 2.2.

Carbon piezoresistive gages were also used on three tests. This gage has much higher sensitivity as compared to manganin. Its sensitivity is reasonably linear at pressures up to 1GPa, however, it is fairly non-linear at higher pressures. An example measurement is shown in Figure 2.3. In this case, the record required unfolding to remove the non-linear effects.

For the rock impact tests, we anticipated pressure requirements on the order of 5GPa. As a result, manganin gages were selected. Additional gage development was done to reduce magnetically induced noise into the gage. This was accomplished by adding a dummy gage whose magnetic induced voltage canceled the magnetic induced voltage in the active gage loop.

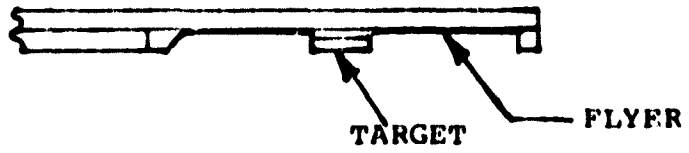

SIDE VIEW

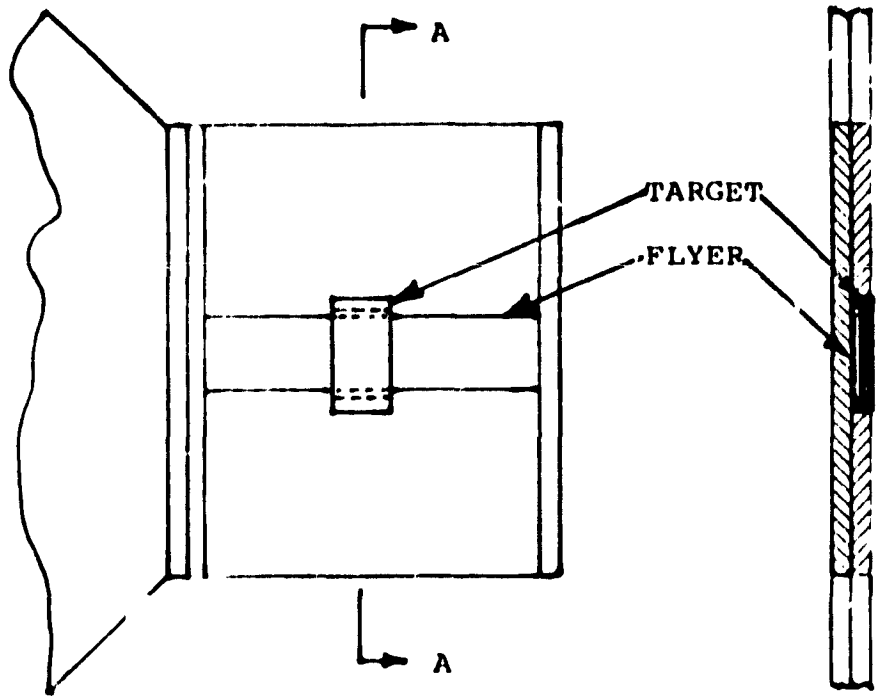

DETAIL A-A

BOTTOM VIEW

SEE FIGURE 8 OF APPENDIX A FOR
FLYER PLATE DETAIL

FIGURE 2.1 FLYER PLATE WITH CALIBRATION FLAT TARGET

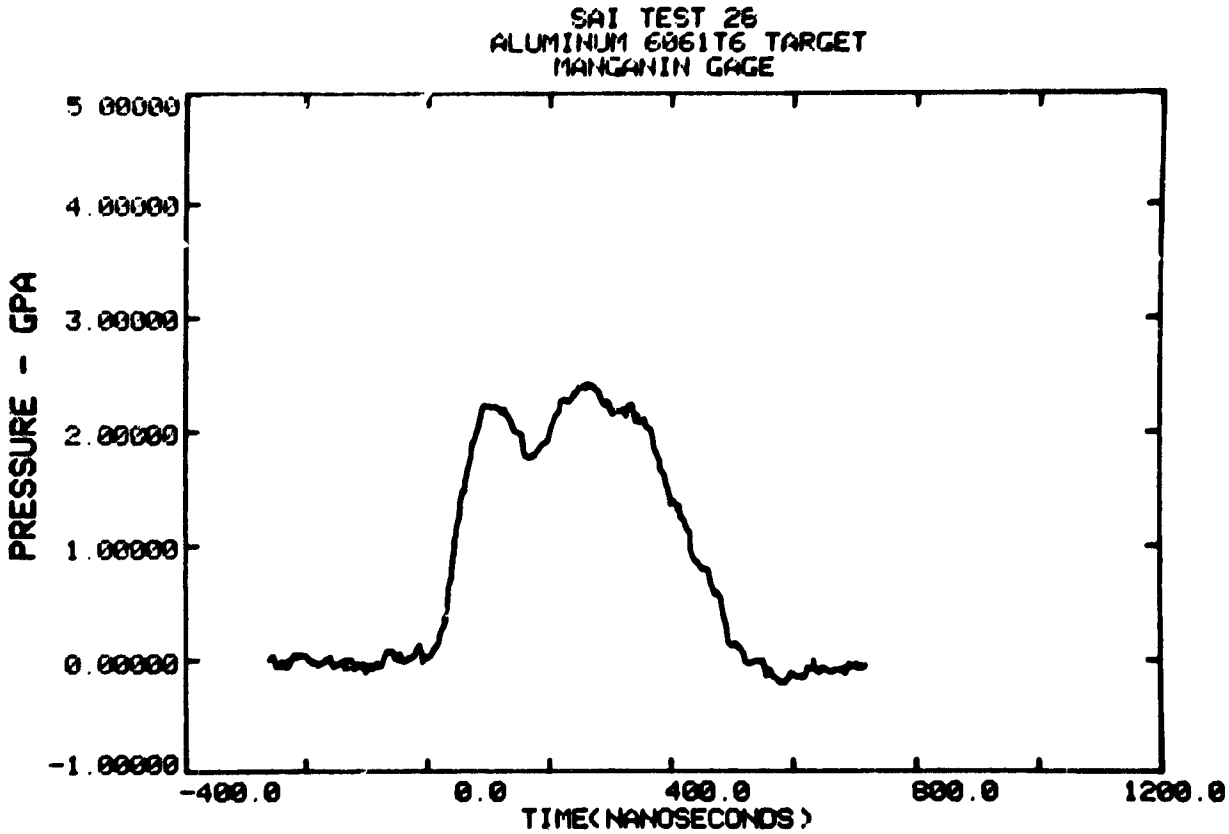

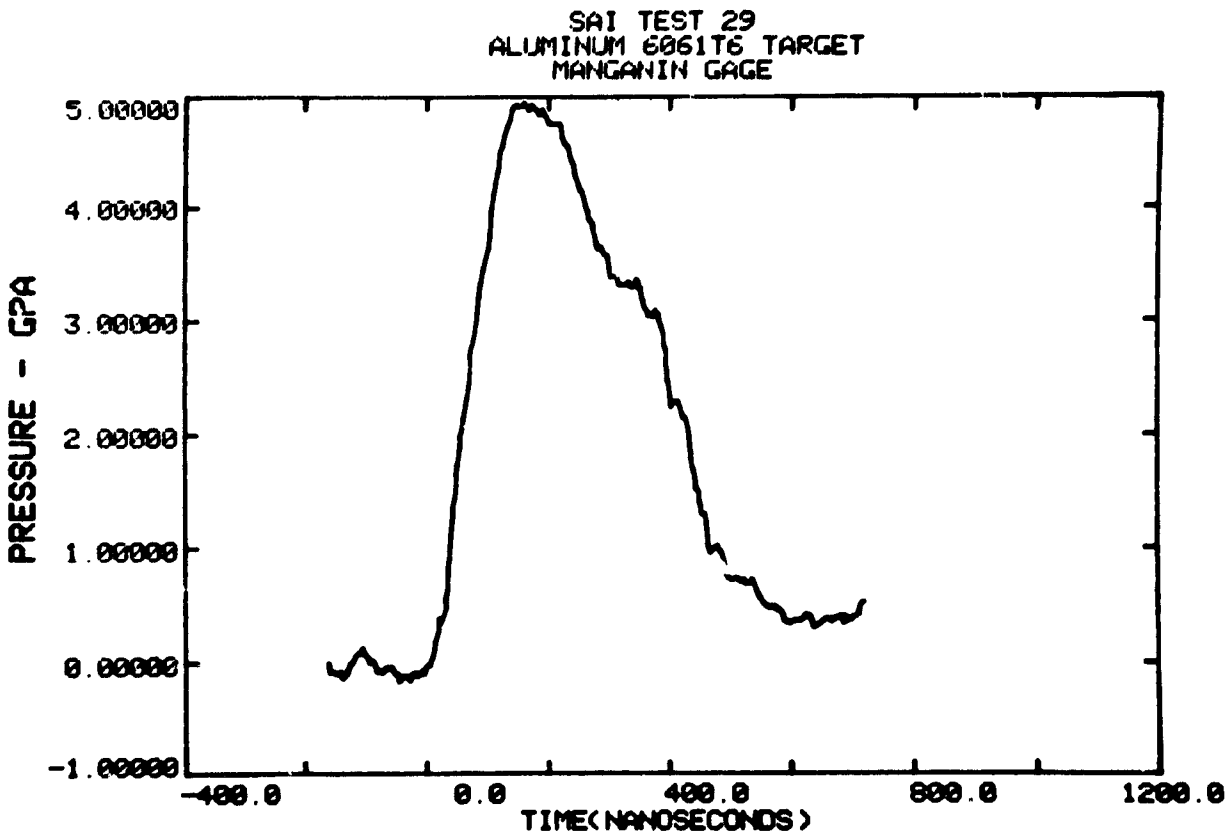

FIGURE 2.2 MANGANIN GAGE CALIBRATION TEST DATA

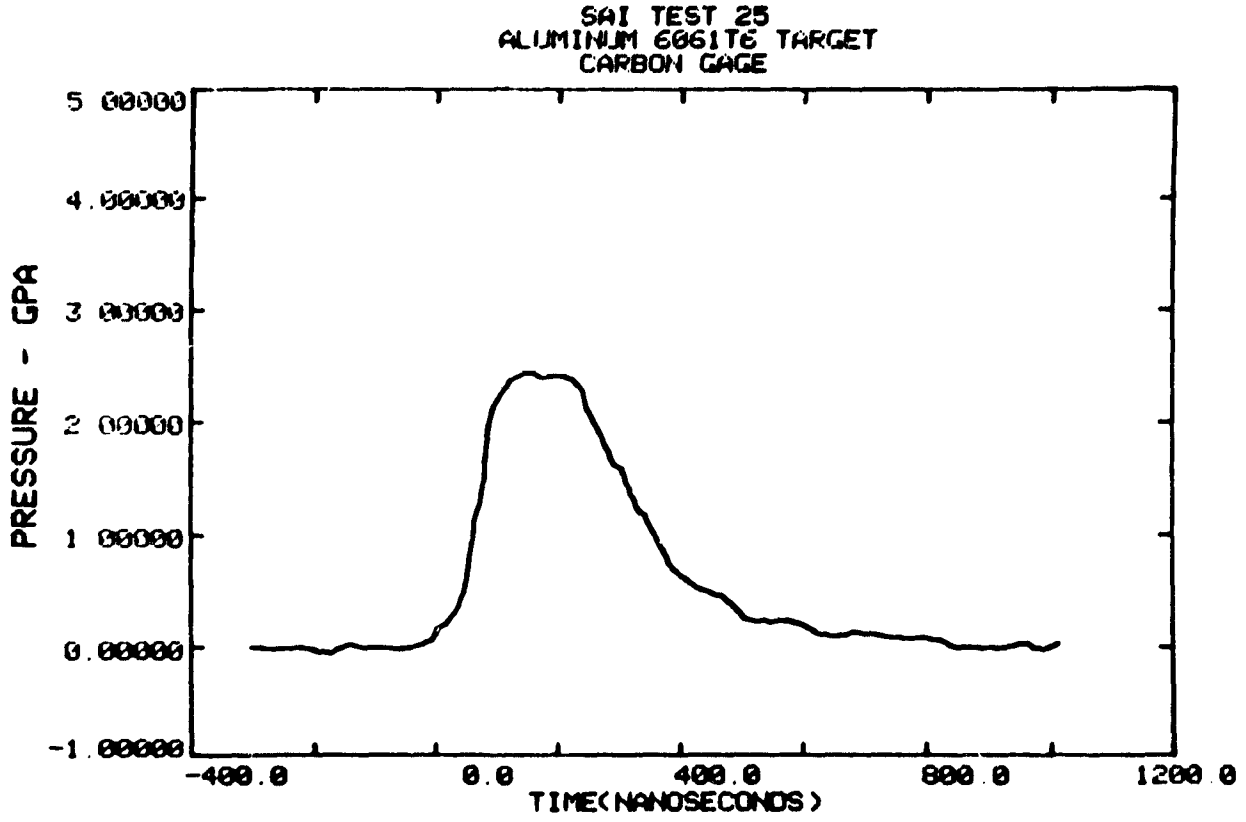

FIGURE 2.3 CARBON GAGE CALIBRATION TEST DATA

3.0 TEST SETUP AND DATA ACQUISITION

A detailed description of the test facility is given in Appendix A. In this section we discuss the flyer plate details, the sample holder and the data acquisition system.

A box was assembled to hold the sample and interface it to the flyer plate. Cross sectional views of the assembly are shown in Figure 3.1. Each sample was imbedded in compacted sand. Sand was selected to provide shock impedance matching to the sample. The box volume was made large compared to the sample in order to minimize shock reflections from the box boundary. The surface of the sample was recessed to provide a 2.54mm (0.10 inch) separation between it and the flyer plate.

The flyer plate was positioned to impact the center of the sample face. The flyer thickness and width were selected to deliver the desired shock pressure for each test sample. The flyer plates were constructed of aluminum sheet stock which had a thickness of 0.508mm (0.020 inch).

Some samples had relatively flat surfaces that were impacted without preparation. Other samples were cut to provide a flat impact surface. In addition, some sample surfaces were filled with an epoxy resin having a density similar to the rock samples.

A sample recording system one-line diagram is shown in Figure 3.2. As listed in Table 1.1, pressure measurements were made in seven samples. The manganin gages were biased by a pulsed power supply located in the screen room. Data were recorded on TEK 7912AD Transient Digitizers. The digitized data were processed by a TEK 4051 Graphics Computer.

Current monitor data were recorded for all sixteen tests. The current monitor signals were used to estimate the peak pressure on each sample. It also was used to trigger the pulse power supplies and the 7912AD's via the Trigger Generator Unit.

Time of arrival data were recorded at four depths in Sample 16. PIN gages were used for this measurement. The PIN signals were mixed and recorded by a TEK 7904 Scope/Camera combination.

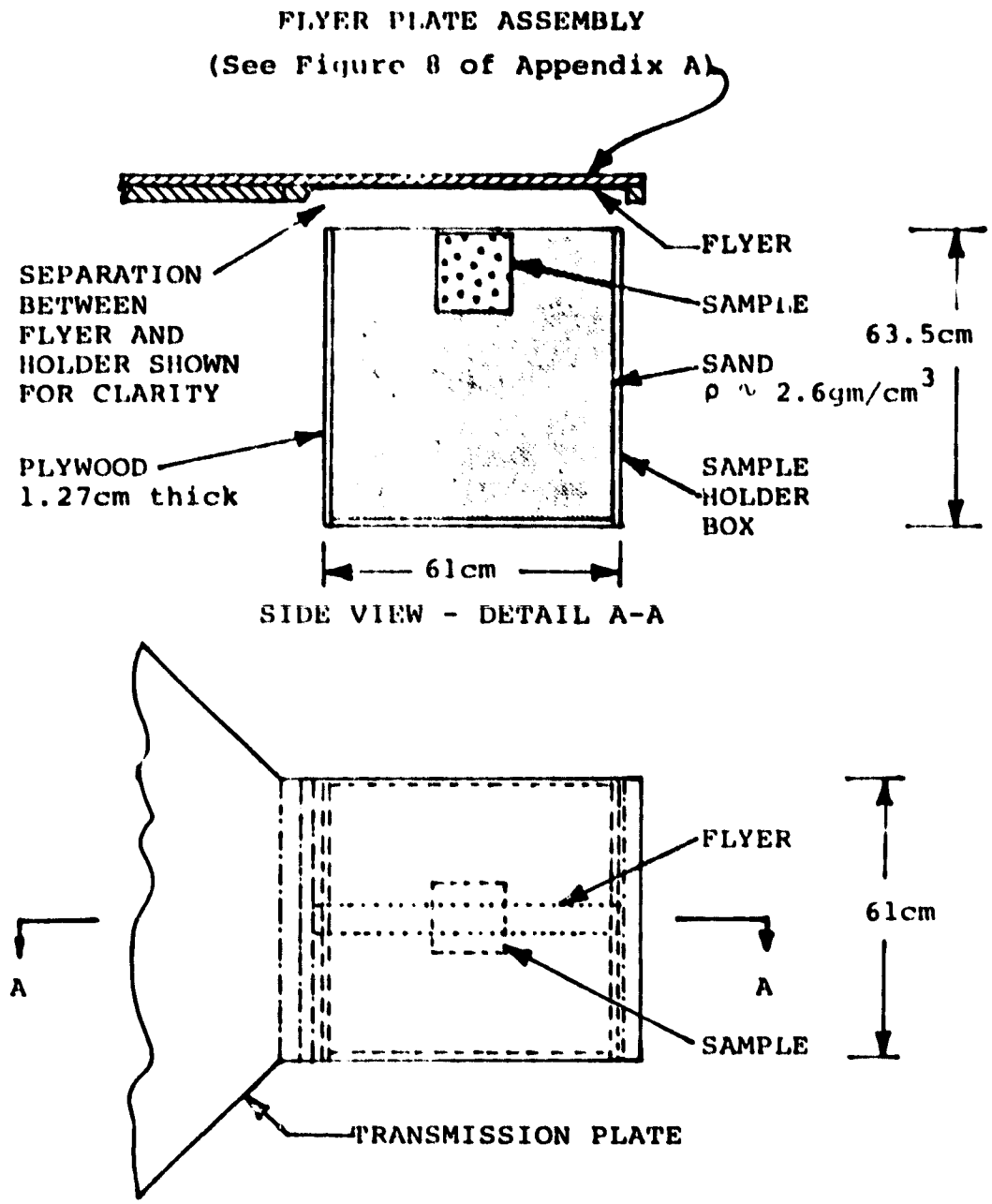

FIGURE 3.1 FLYER PLATE AND SAMPLE HOLDER ASSEMBLY

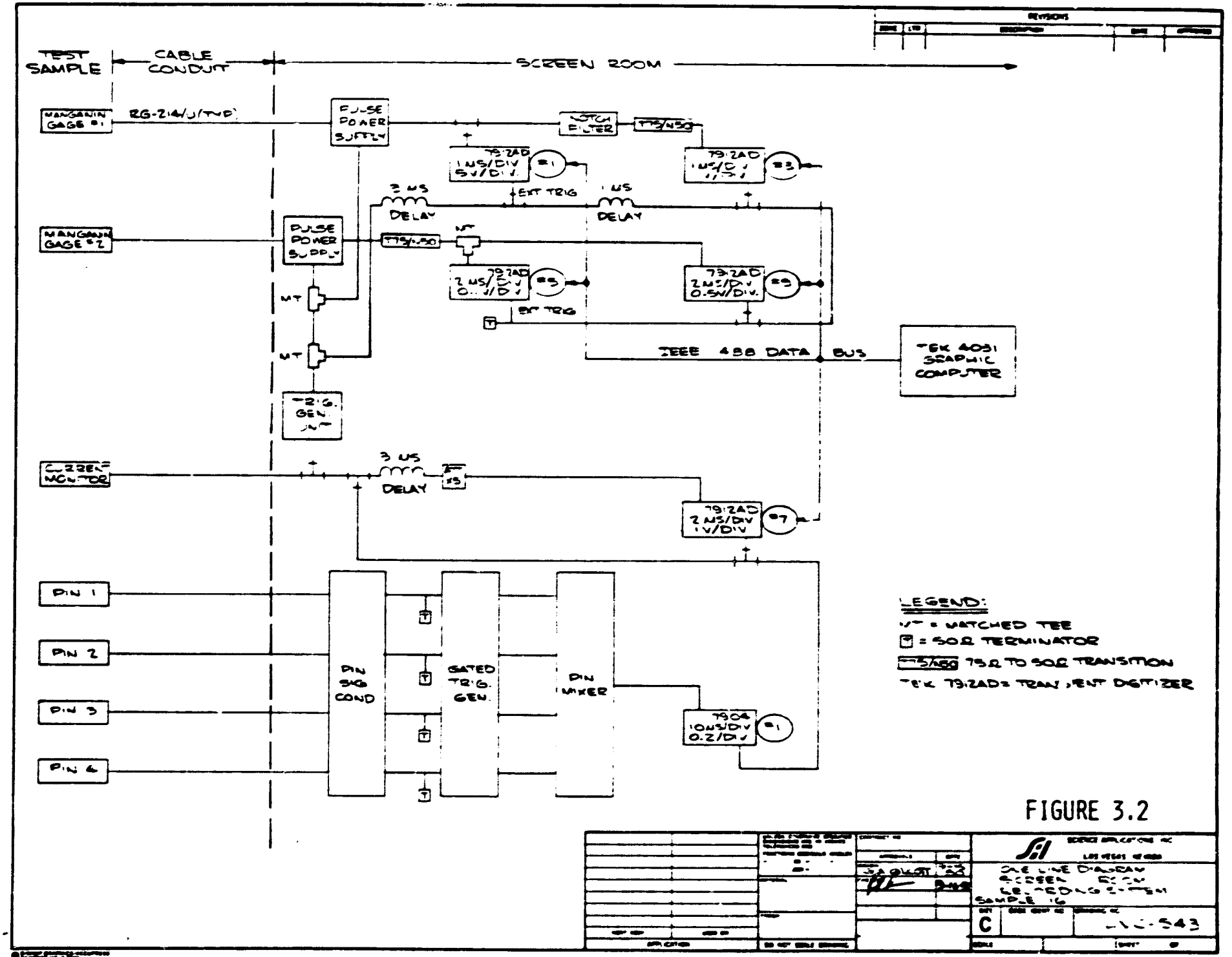
TEST SAMPLE
CABLE CONDUIT
SCREEN ROOM
MANGANIN GAGE #1
RG-214/U(TYP)
PULSE POWER SUPPLY
NOTCH FILTER
79:2AD 1 MS/DIV 5V/DIV #1
79:2AD 1 MS/DIV #3
EXT TRIG
3 MS DELAY
1 MS DELAY
MANGANIN GAGE #2
PULSE POWER SUPPLY
MT
79:2AD 2 MS/DIV 0.5V/DIV #5
79:2AD 2 MS/DIV 0.5V/DIV #9
EXT TRIG
MT
MT
T.G. GEN. #4
IEEE 488 DATA BUS
TEK 4051 GRAPHIC COMPUTER
CURRENT MONITOR
3 MS DELAY
#6
79:2AD 2 MS/DIV 1V/DIV #7
PIN 1
PIN 2
PIN 3
PIN 4
PIN SIG COND
GATED TRIG. GEN.
PIN MIXER
7904 10MS/DIV 0.2/DIV #1
LEGEND:
MT = MATCHED TEE
= 50Ω TERMINATOR
75Ω TO 50Ω TRANSITION
TEK 79:2AD = TRANSIENT DIGITIZER

FIGURE 3.2

4.0 TEST DATA

Active pressure measurements were made in seven samples. The peak recorded pressures are listed in Table 1.1. Current monitor measurements were recorded on all tests. The current monitor records the current flowing in the flyer plate. The initial signal peak may be used to estimate the flyer velocity and thus, the peak pressure delivered to the sample. The current monitor wave shape also is used to verify proper capacitor bank performance. An example wave shape is shown in Figure 4.1.

Samples 1, 2, 3, 4 and 6 were concrete compositions that were tested. The pressure record for Sample 1 is shown in Figure 4.2. The peak pressure for this record is much greater than predicted. For all of the concrete samples tested, there was very little fracturing at depth. The surface was pulverized to powder to a few millimeters depth. The samples also were driven up to 2cm into the sand. The pressure records show a stepped rise front, indicating the impact pressure was reflected at near surface and thus, did not propagate through the sample. The result is that the impact energy was converted to thermal energy at the surface plus momentum that drove the sample into the sand. The gage record also shows evidence of strain. The trailing edge of the pressure pulse does not return to the initial zero pressure level. This indicates that the gage was deformed during strain that, we postulate, occurred during the reflected shock.

The limestone and plexiglass samples were fractured to varying degrees. In most cases, there was evidence of surface thermal damage, but there was little evidence of samples being driven into the sand. The result is that most of the shock energy propagated into the sample and was dissipated as fracture energy. In most cases, there was severe damage at the bottom of the sample. This indicates that the impedance between the sample and the sand was not well matched. Pressure records

for two samples are shown in Figure 4.3. The pulse shape for Test 49 is about as expected, indicating that the shock impedance between the flyer, the sample and the gage was pretty good. For Test 47, the pulse shape is longer and has lower amplitude than expected. We suspect that the epoxy filler in the gage assembly was not properly cured. Its shock response was slower as indicated by the slow pulse rise time. Although the peak shock is less than expected, the total energy is as predicted.

On the final test sample (No. 16), we attempted to measure the shock velocity through the rock and the pressure attenuation as a function of depth. We recorded pressure at two depths as indicated in Table 1.1. The shock time of arrival (TOA) was recorded by PIN gages that were imbedded at four depths. The resultant TOA data are graphed in Figure 4.4. The test sample and gaging sequence photographs are shown in Figure 4.6. Only three of the PIN gages closed. This is possibly because the pressure at depth was less than expected for this test. In Figure 4.5, we graph shock pressure versus depth for the limestone sample. This plot is based only on the two data points obtained on this test. Its accuracy is questionable until other data are gathered.

The flat flyer plate generated a planer shock wave. On some tests we found that the edges of the flyer were curling which caused a shear wave where the edge impacted the sample. This was noticeable when the 5.08mm (2 inch) wide flyer was used. The wider flyers did not show evidence of significant curling.

On Sample 10, we attempted to generate a point source shock wave. The sample was covered with a sheet of teflon 6.35mm (0.25 inch) thick. A 12.7mm (0.5 inch) diameter aluminum slug was inserted in the telfon at the center of the sample. The purpose of this arrangement was to attenuate the flyer shock in the teflon, while coupling shock through the aluminum slug which was in contact with the sample. This setup appeared

to work well. Examination of the sample showed no evidence of the edge curl shear wave. There was an impression of the aluminum slug at the sample surface. The teflon showed severe damage by the flyer edge. The teflon was nearly severed along the edge lines. The edge zone was also blackened from joule heating.

Sample 11 was constrained in an attempt to limit the severity of fracturing that was seen on previous samples. For this sample, we epoxy bonded 6.35mm (0.25 inch) aluminum sheet stock around the sides. There was no aluminum on the top or bottom surfaces. The side plates then were banded to generate static pressure that would counteract the internal radial fracturing. The sample showed some evidence of surface fracturing and the bottom was sheared off at about 2cm height. At the time of this writing, the sample has not been broken open to examine the internal damage.

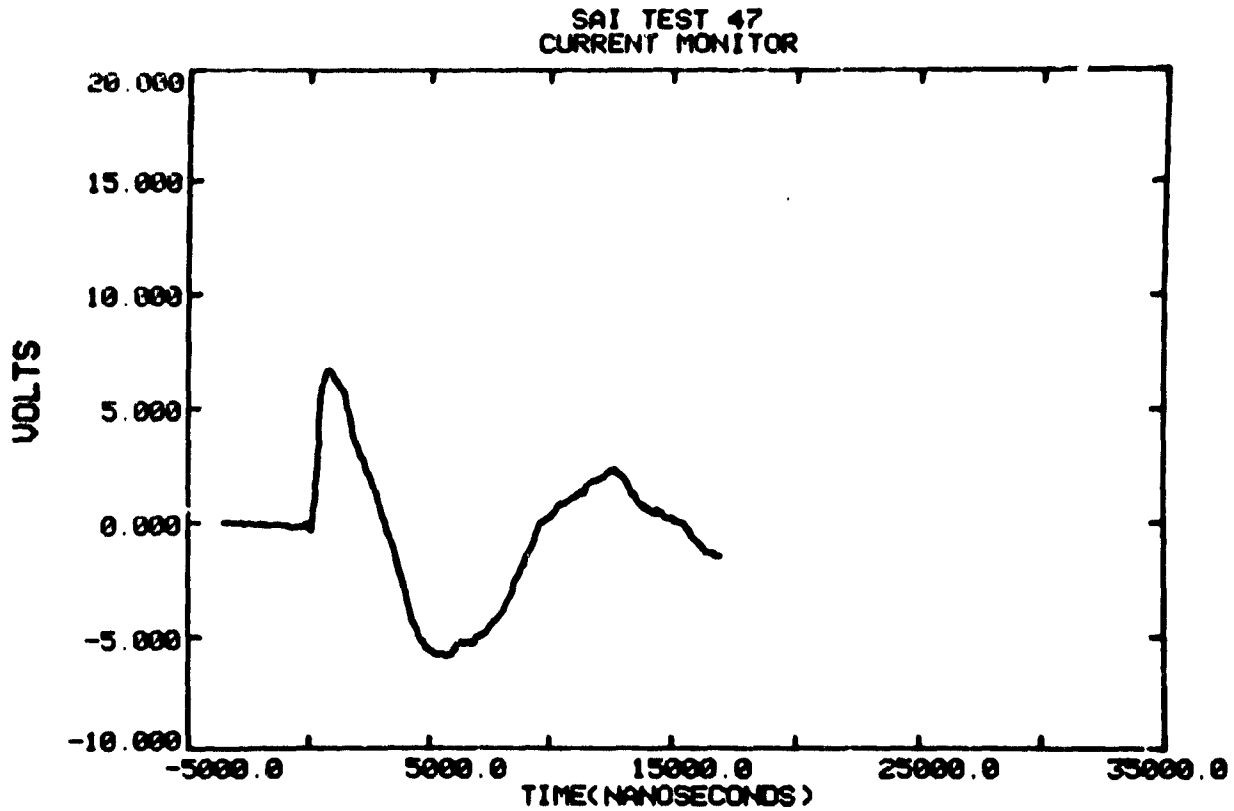

FIGURE 4.1 CURRENT MONITOR RECORD

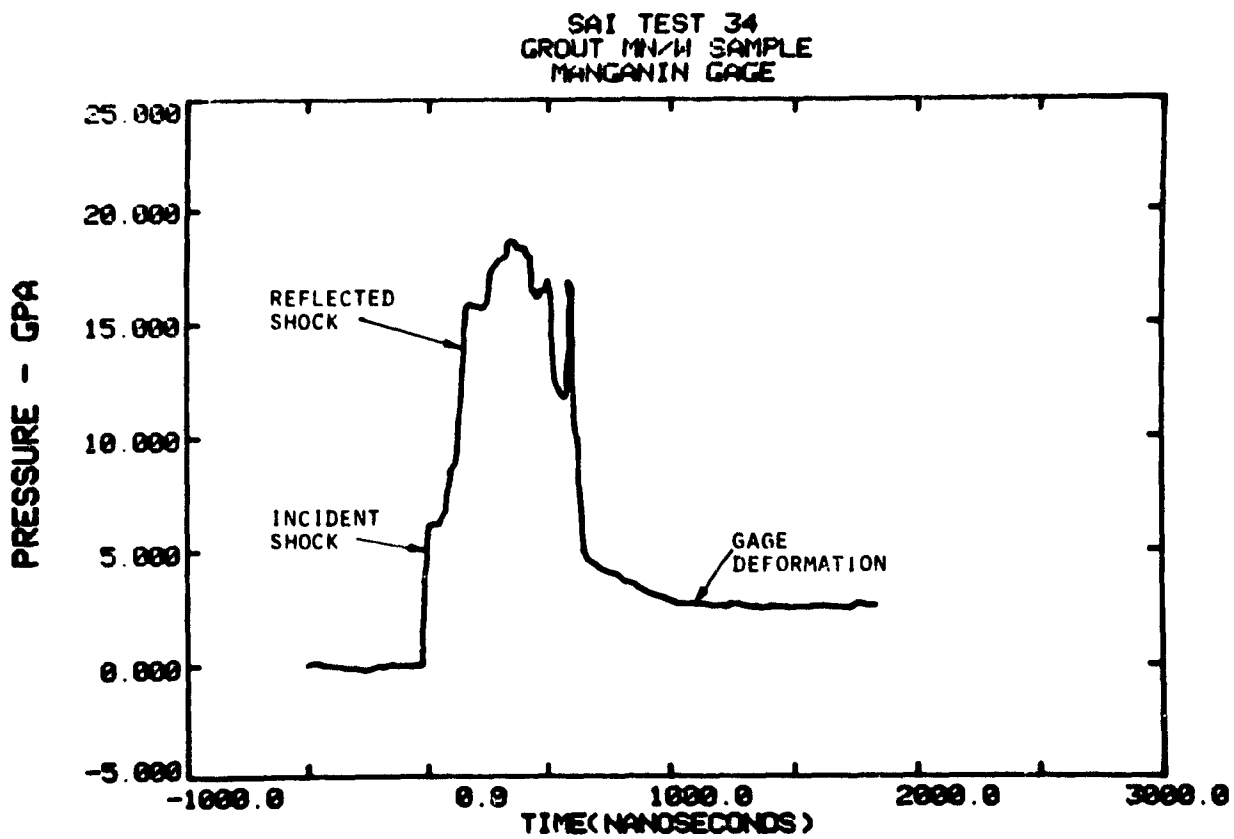

FIGURE 4.2 GROUT SAMPLE PRESSURE RECORD

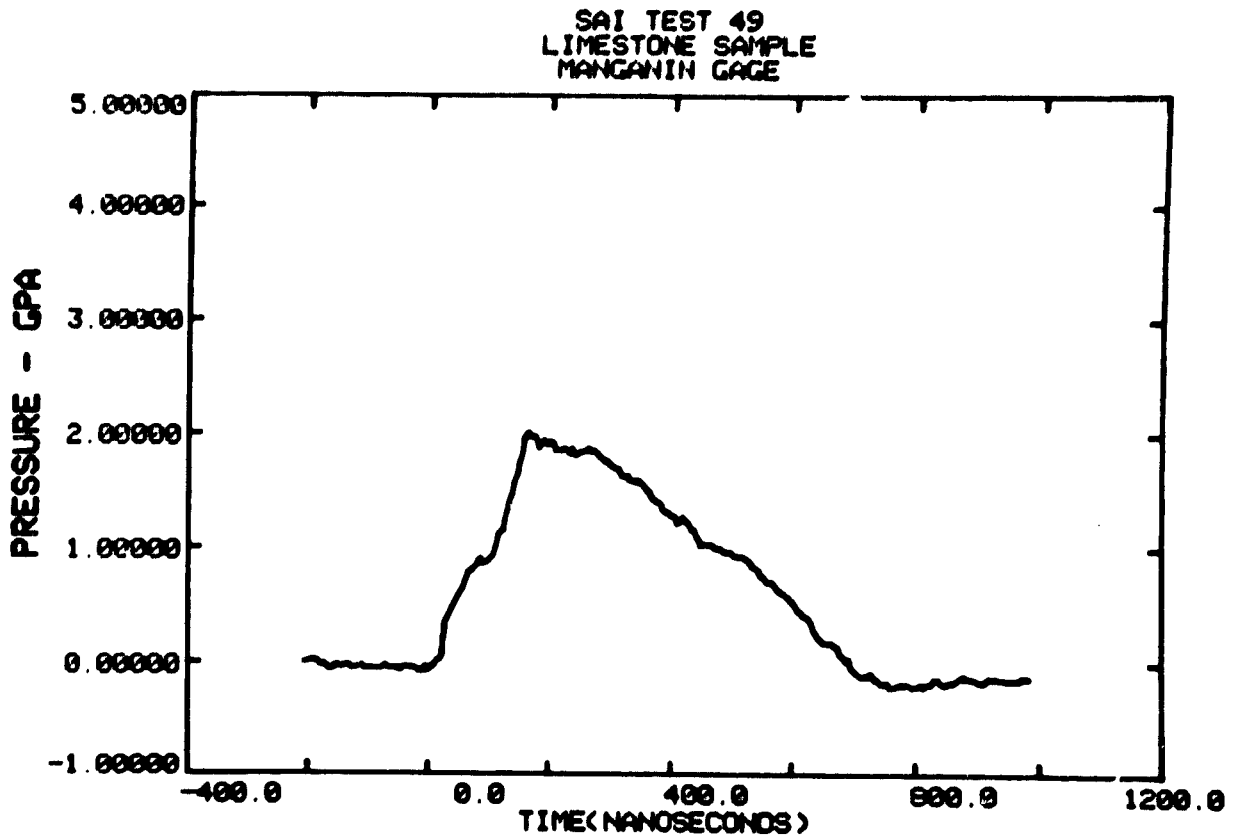

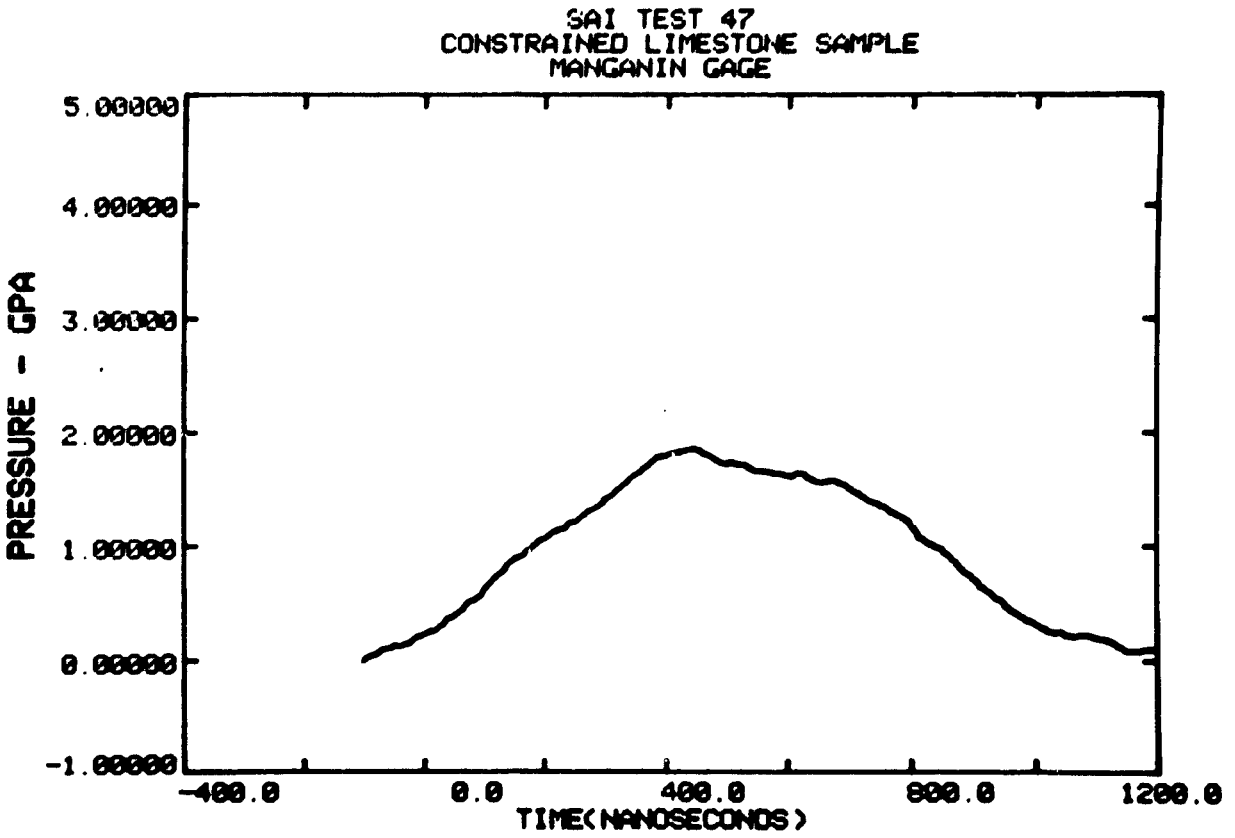

FIGURE 4.3 LIMESTONE SAMPLE PRESSURE RECORDS

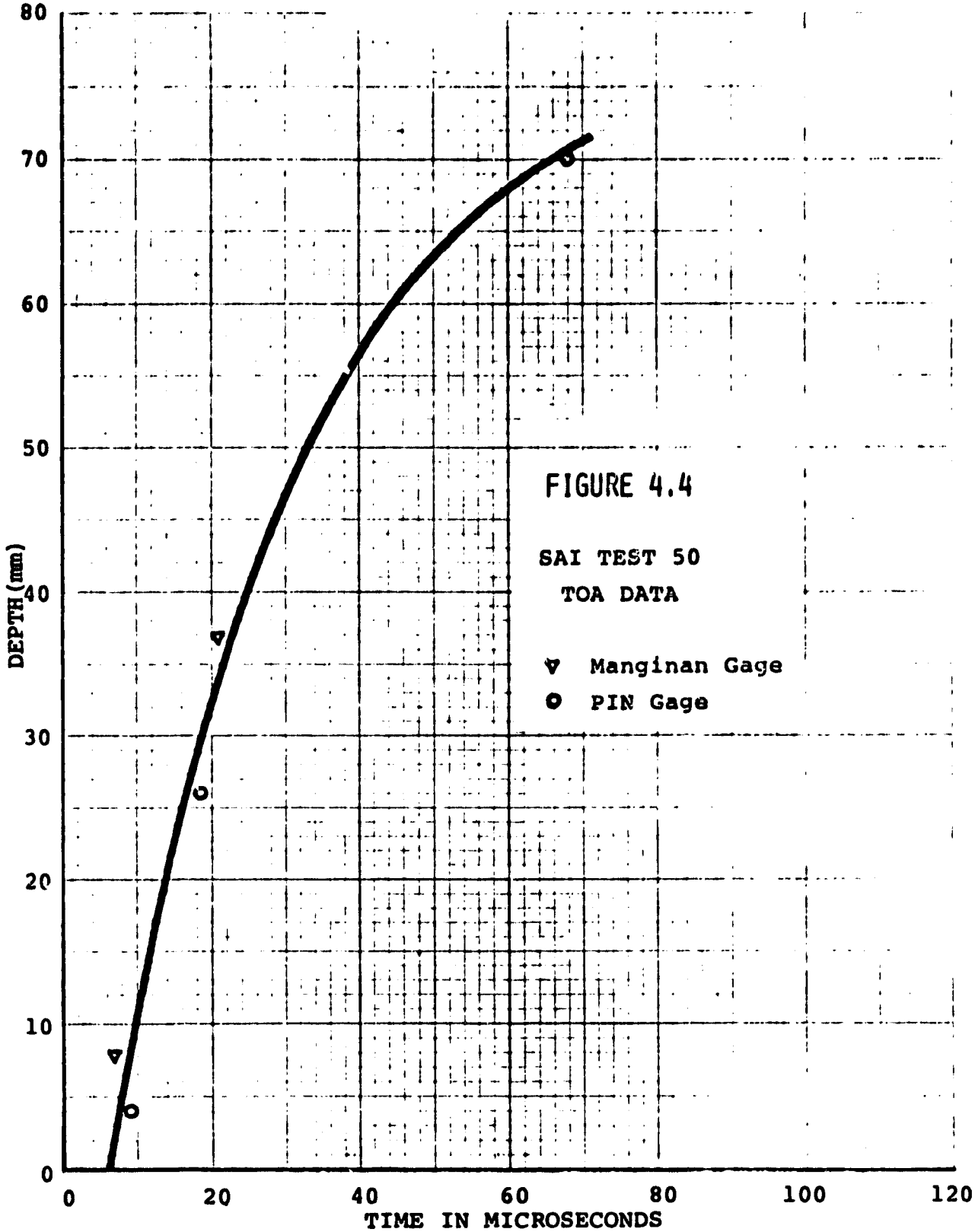

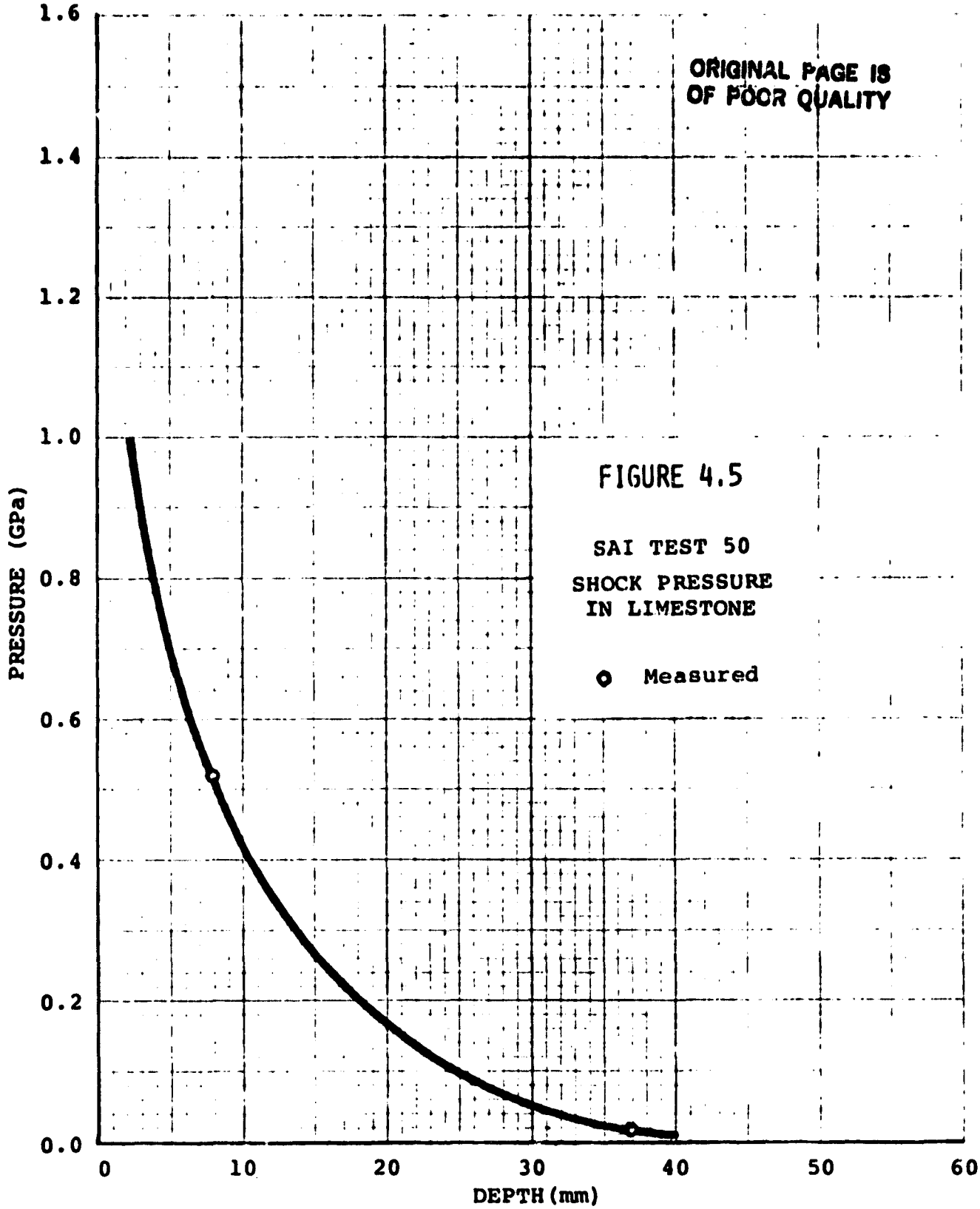
ORIGINAL PAGE IS
OF POOR QUALITY
FIGURE 4.5
SAI TEST 50
SHOCK PRESSURE
IN LIMESTONE
Measured
PRESSURE (GPa)
1.6
1.4
1.2
1.0
0.8
0.6
0.4
0.2
0.0
0
10
20
30
40
50
60
DEPTH (mm)

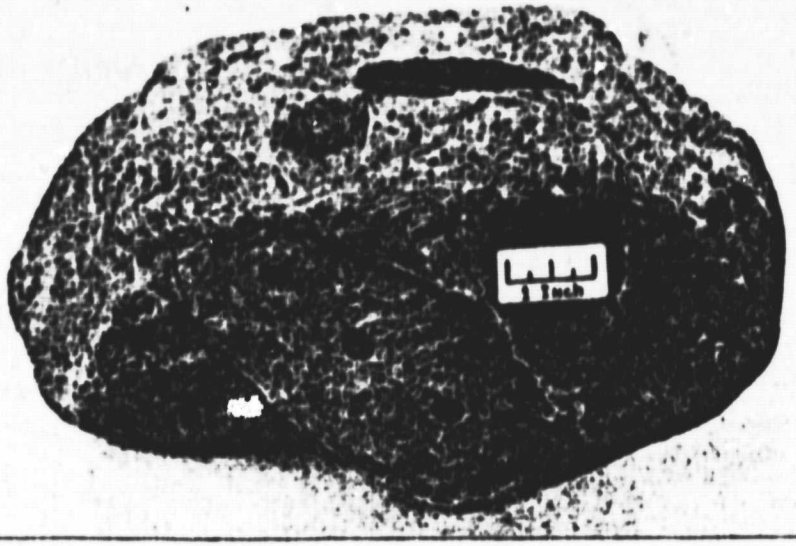

FIGURE 4.6A LIMESTONE SAMPLE PREPARED FOR GAGE INSTALLATION

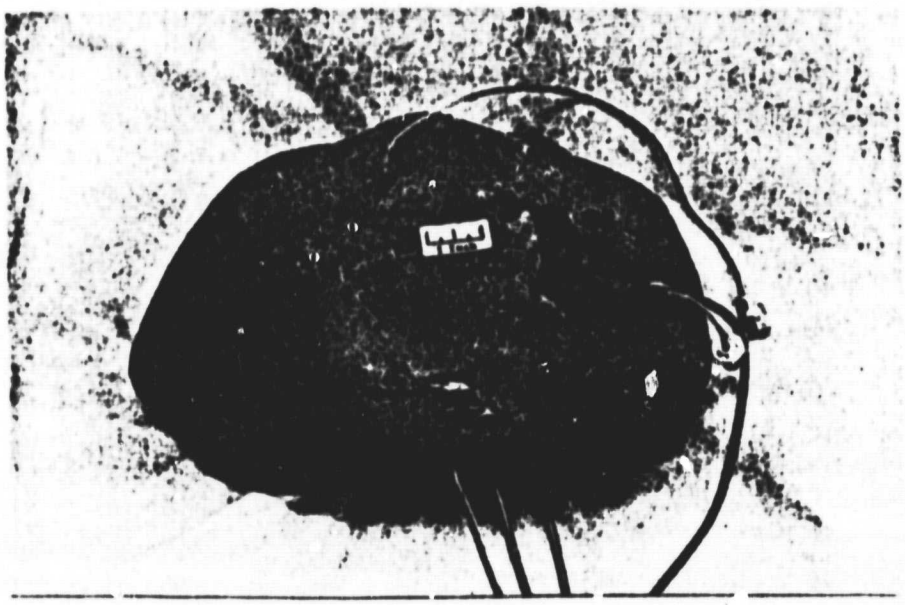

FIGURE 4.6B GAGES INSTALLED

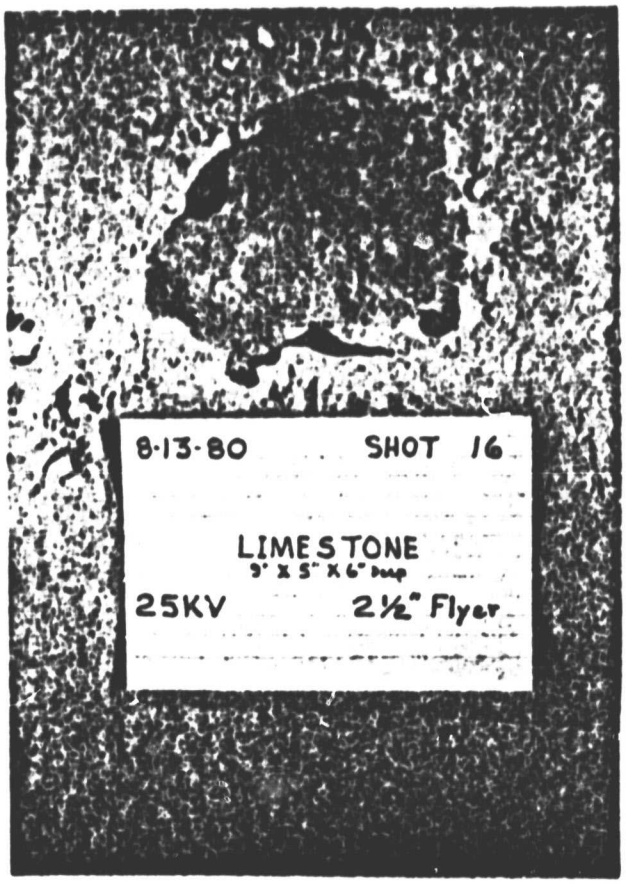

FIGURE 4.6C SAMPLE
INSTALLED IN HOLDER

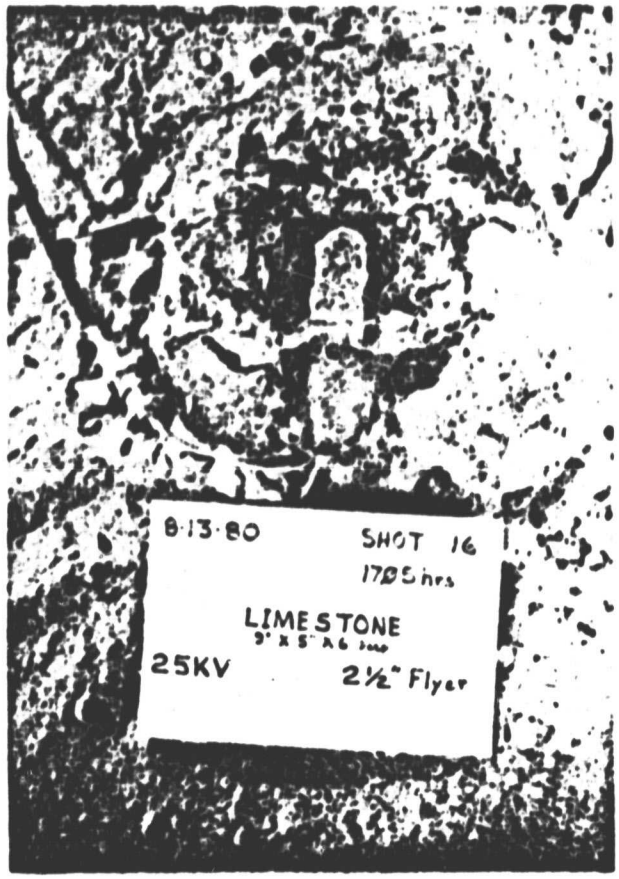

FIGURE 4.6D SAMPLE
AFTER IMPACT

5.0 CONCLUSION

The magnetically driven flyer plate appears to be a good method for investigating rock fracture mechanics under laboratory conditions. The flyer can generate a high stress planer shock wave over a relatively large area. Gaging techniques have been developed to successfully measure the dynamic pressure and shock time of arrival in rock while minimizing the induced effects of the flyer plate's magnetic fields.

At the time of this writing, the limestone samples have not been fully examined to determine if shatter cone fracture formations have been created. Cursory examination of several samples show fracturing that appears to contain the mechanisms that cause shatter cones. Detailed analysis of the samples is being done by Linnerude and Roddy. They will report their findings in separate documentation.

A review of the data obtained during this test series indicates the desirability to do additional testing. We recorded data to determine shock velocity and attenuation in one sample. Additional samples should be tested to validate and expand on these data. The analysis of Linnerude and Roddy may also point up the need for follow up work. This work may involve rerunning tests that were done during this series to check repeatability; or some test perameters may be changed, such as, larger flyer plates and/or higher shock pressures.

APPENDIX A

A HIGH ENERGY CAPACITOR BANK IMPACT FACILITY

SCIENCE APPLICATIONS, INCORPORATED
3351 S. HIGHLAND DRIVE, SUITE 206
LAS VEGAS, NV 89109
(702)732-0108

A HIGH ENERGY CAPACITOR BANK IMPACT FACILITY

The SAI Las Vegas laboratory operates a high energy capacitor bank that is used to magnetically drive flyer plates for impact studies. The purpose of such studies is to evaluate the performance of materials and structures when subjected to impulsive surface loading that may reveal damage levels and failure modes.

The capacitor bank (Figures 1 and 2) has four modules each containing 24 Maxwell low-inductance capacitors that are rated at 60 kilovolts. The average capacitance of the 96 capacitors is 2 microfarads which allows a maximum stored charge of 346 kilojoules. The four-module system can be operated with one to four modules with a charge range of 10 to 60 kilovolts, thus offering a stored energy range of 2.4 to 346 kilojoules (Figure 3).

All bank switching is accomplished with solid dielectric switches. Each module contains one switch which is triggered from a common trigger generator capable of supplying a synchronous trigger to as many as four modules. While the desired operating voltage seems to be the range of 15 to 45 kilovolts, an estimated 60 to 75 firings have been conducted with four modules and operating voltages between 52 and 58 kilovolts. Even though individual capacitors have been hi-potted to 70 kilovolts and discharged into a short circuit as an acceptance test, the maximum charge voltage to date has not exceeded 58 kilovolts.

The Las Vegas facility is capable of handling large test objects as well as supporting instrumentation such as streak cameras. The facility is contained in 6400 square feet of floor space which includes a machine shop, assembly areas and a control room. Instrumentation includes oscilloscopes and a 24-channel

strain gage system that is permanently wired to the capacitor bank room. The Las Vegas lab includes a double shielded instrumentation screen room with shielded cable conduits routed to the capacitor bank room. The capacitor bank is enclosed in an electromagnetically shielded room to reduce noise propagation.

Data are recorded by equipment located within the screen room such as shown in Figure 4. The discharge ringing frequency into a short circuit for the four module system is 225 kHz, based on the first full half cycle from the DI/DT sensors. Typical diagnostics records are shown in Figure 5. Flyer plate velocity typically is recorded by a streak camera viewing the edge or center of the flyer plate. Example streak records are shown in Figures 6 and 7.

A discussion of the magnetic flyer technique is given in the following section. SAI is currently conducting flat target tests where the peak surface target pressure must be known. SAI is developing a piezoresistive pressure gage technique using manganen and carbon gage elements. This will result in direct pressure measurements; however, at low pressures the gages are subject to pickup of electromagnetic noise generated during bank discharge. An indirect measurement of pressure may be derived from a streak camera record of the flyer motion. From a measurement of the flyer velocity v_f, the front surface peak pressure P_o follows from the relation

$$P_o = v_f \frac{Z_f Z_t}{Z_f + Z_t}$$

where Z denotes the shock acoustic impedance of the flyer (f) or target (t) material. The shock pulse width is comparable to the round trip shock propagation time within the flyer. Present tests involve 20 mil thick aluminum flyers that generate peak pressures of 50 to 100 kilobars at a pulse width of about 0.3 microseconds. An illustration of a flat plate flyer assembly is shown in Figure 8.

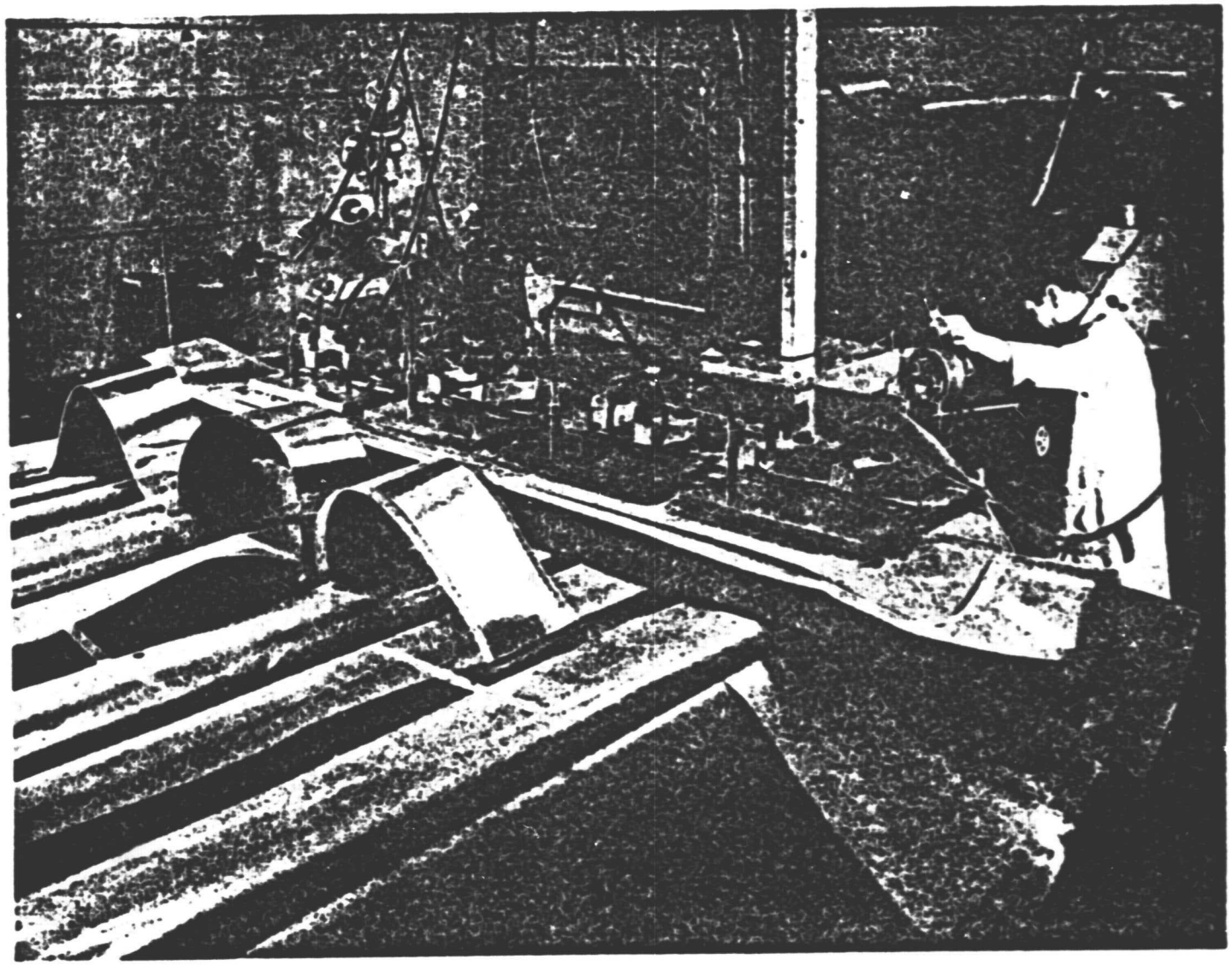

FIGURE 1. PHOTOGRAPH SHOWING FRONT OF CAPACITOR BANK WITH LOAD BLOCK, STREAK CAMERA AND XENON FLASH, AND FAST FRAMING CAMERA.

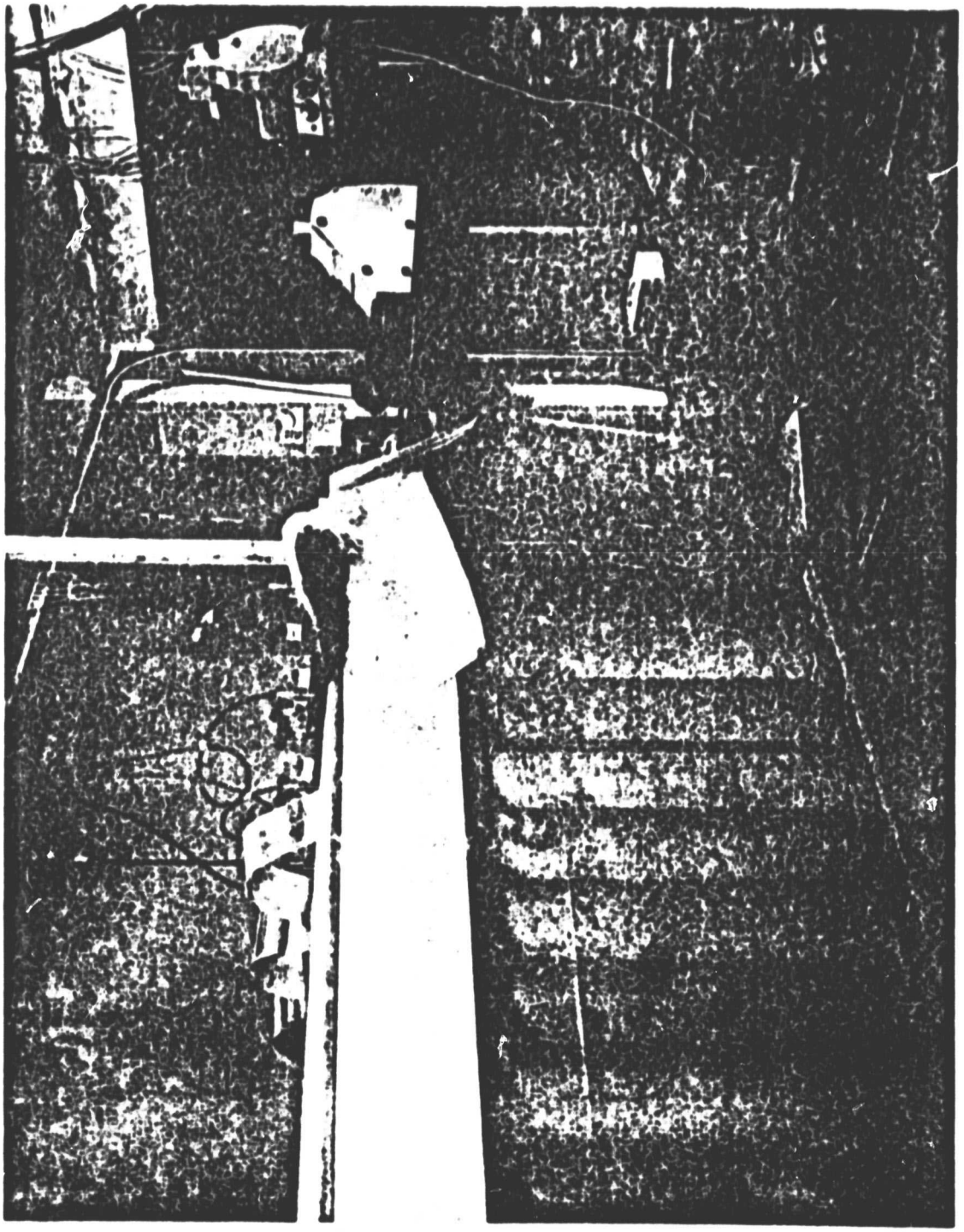

FIGURE 2. SIDE VIEW OF CAPACITOR BANK AND PHOTOGRAPHIC INSTRUMENTATION.

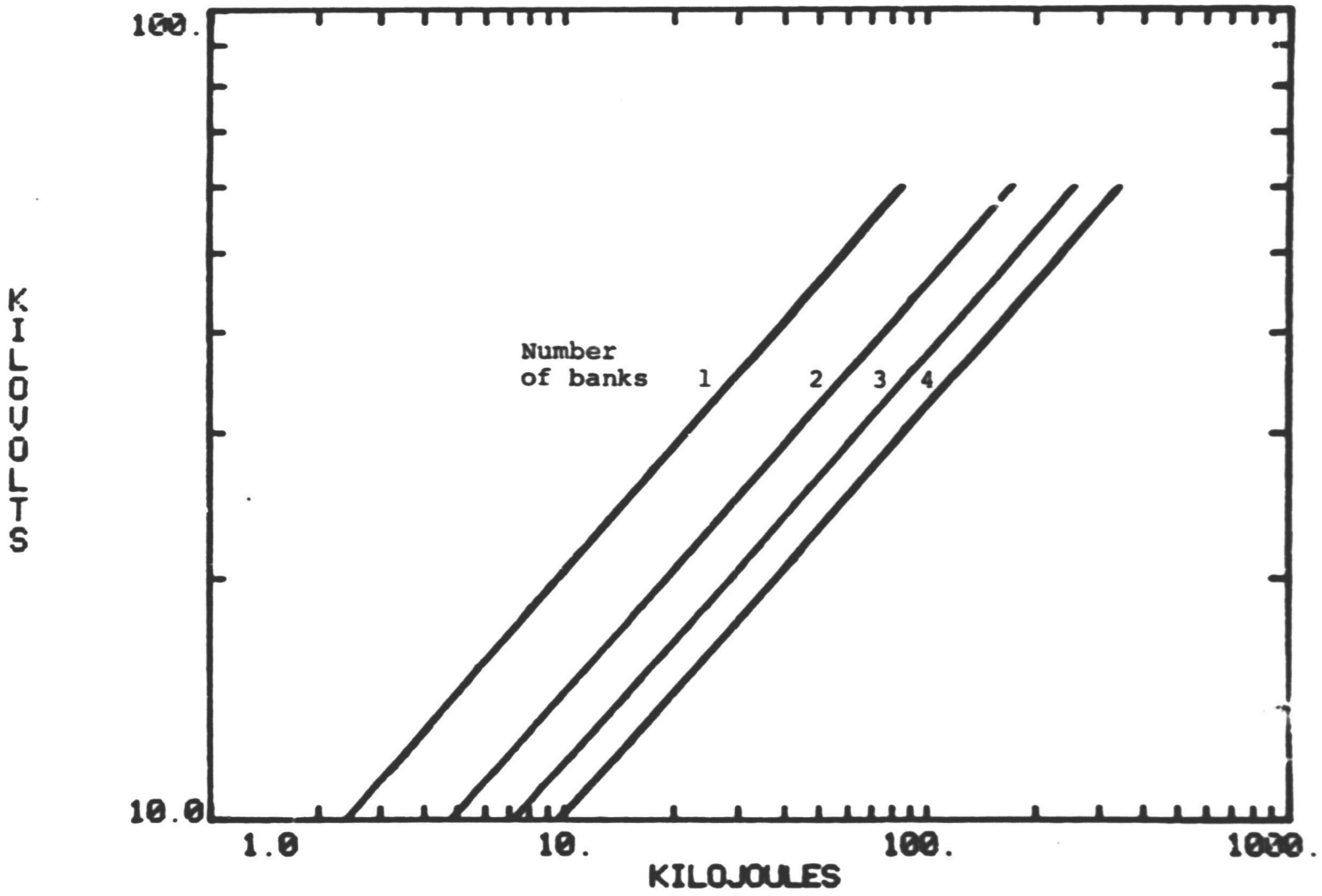

FIGURE 3. BANK ENERGY VS. VOLTAGE

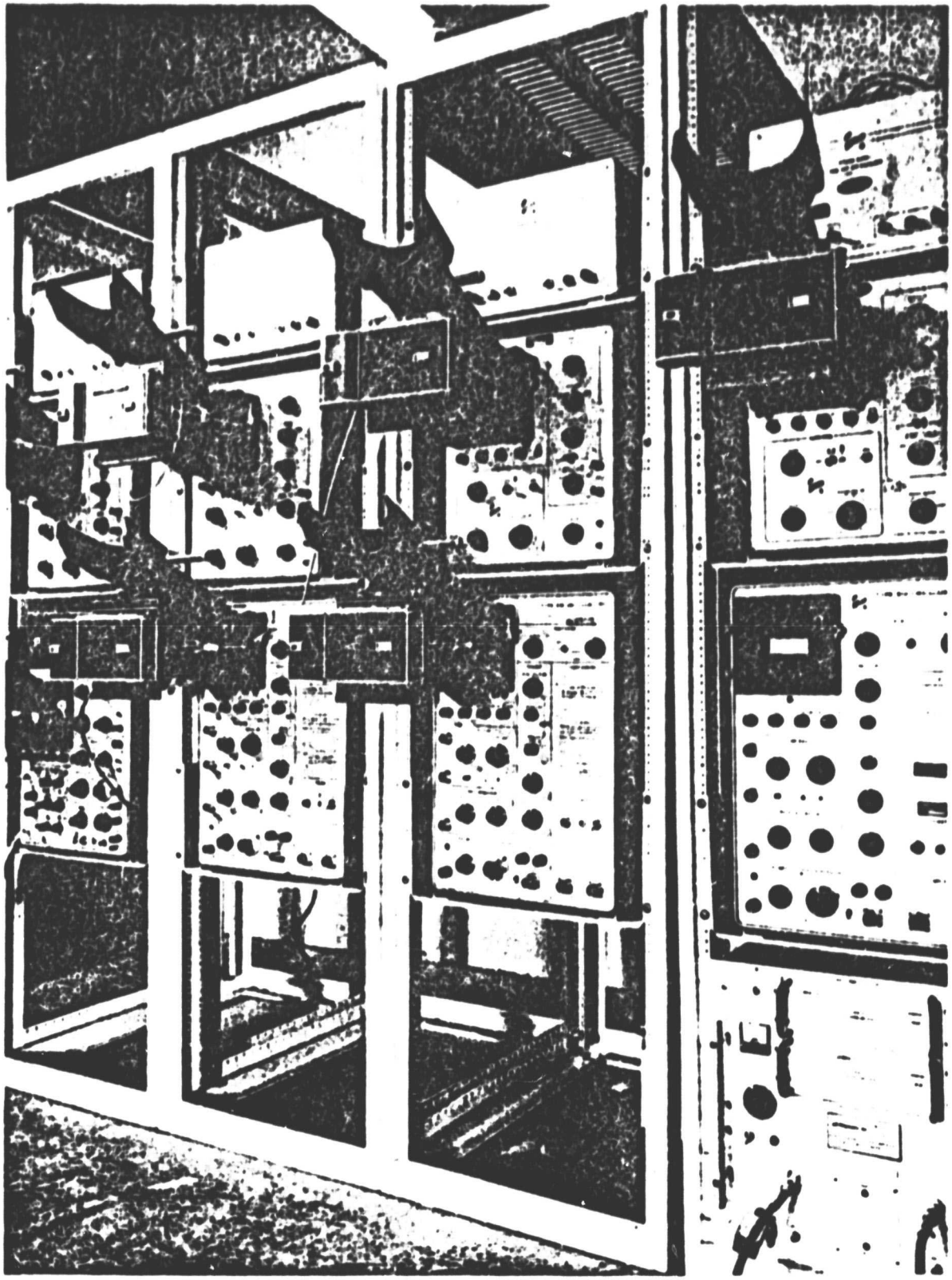

FIGURE 4. DIAGNOSTIC OSCILLOSCOPES USED IN MONITORING CAPACITOR BANK PERFORMANCE DURING BANK FIRING.

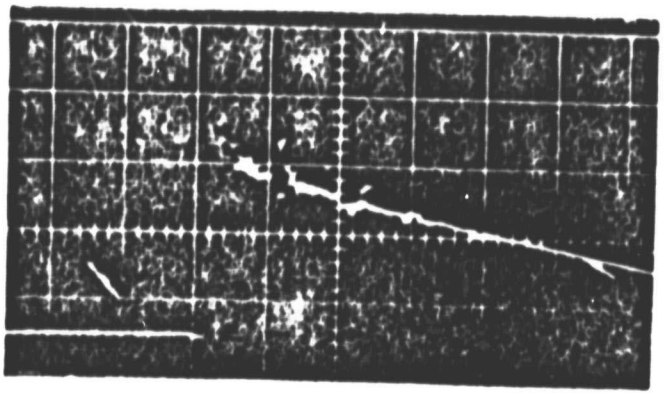

a) Fast dI/dt, 200 ns/div

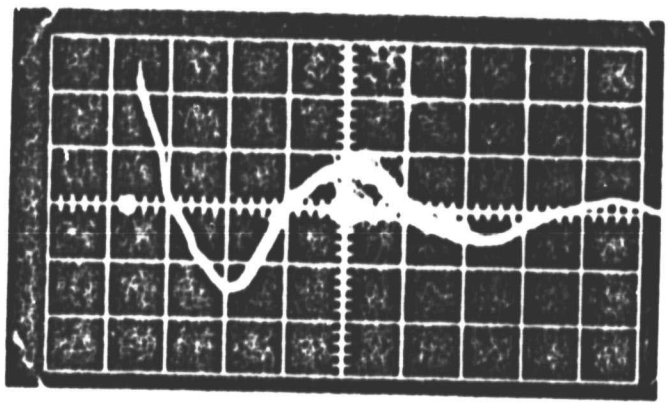

b) Normal dI/dt, 2 μsec/div

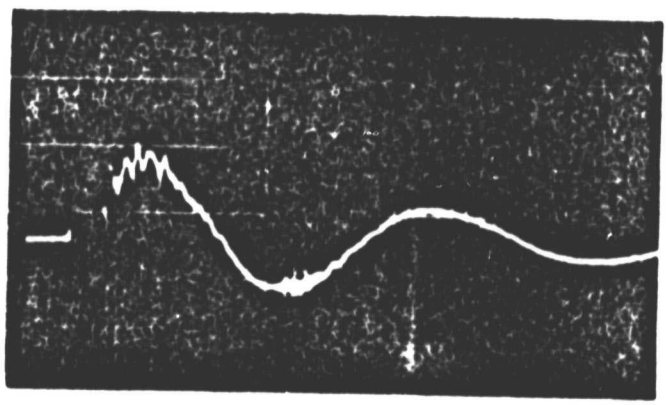

c) Current I, 2 μsec/div

FIGURE 5. TYPICAL BANK DIAGNOSTIC TRACES.

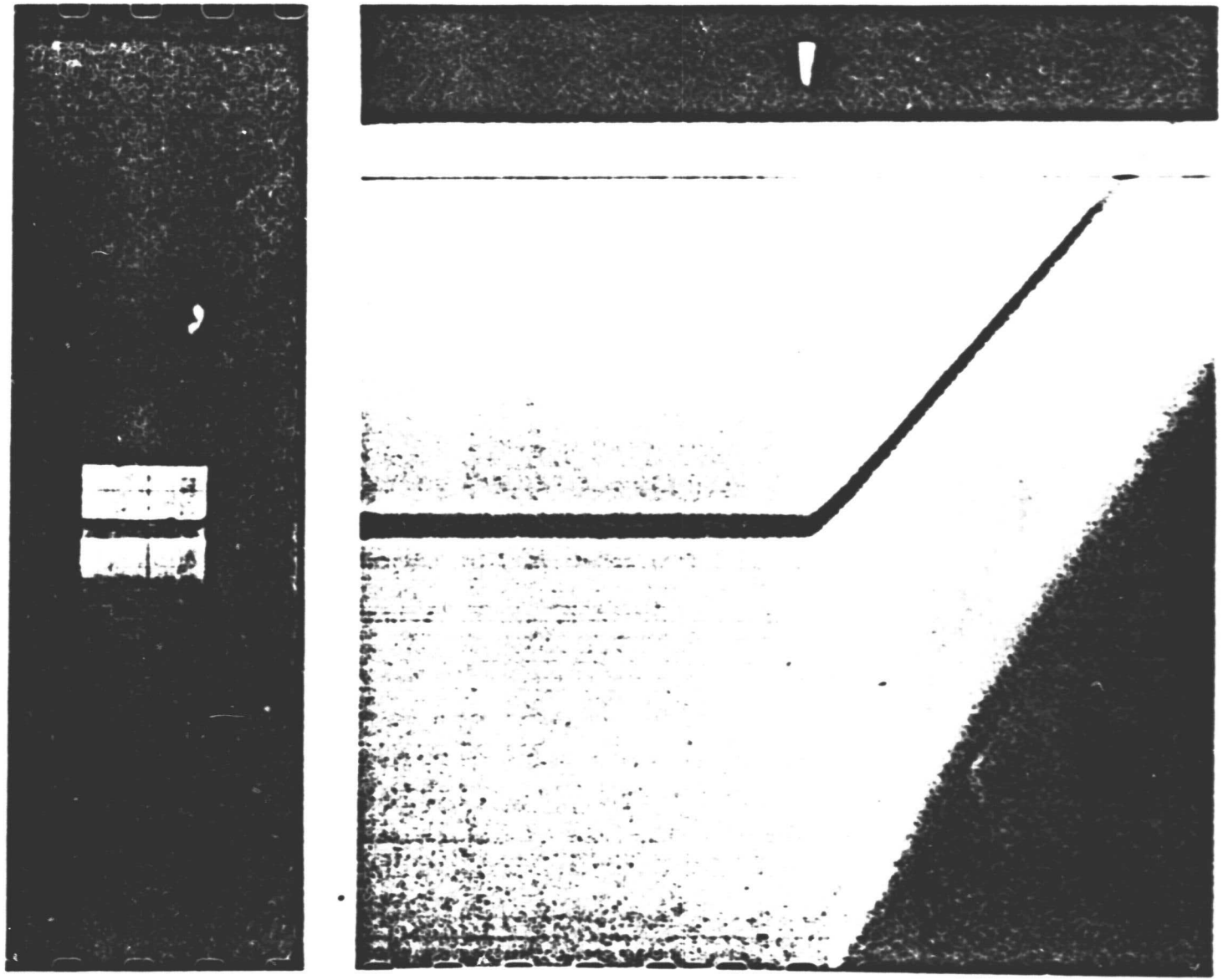

FIGURE 6. TYPICAL STREAK RECORD OF CENTERLINE FLYER VELOCITY SHOWING DIMENSIONAL STANDARD AND BANK FIRE FIDUCIAL.

FIGURE 7. STREAK RECORD OF CENTERLINE FLYER VELOCITY.

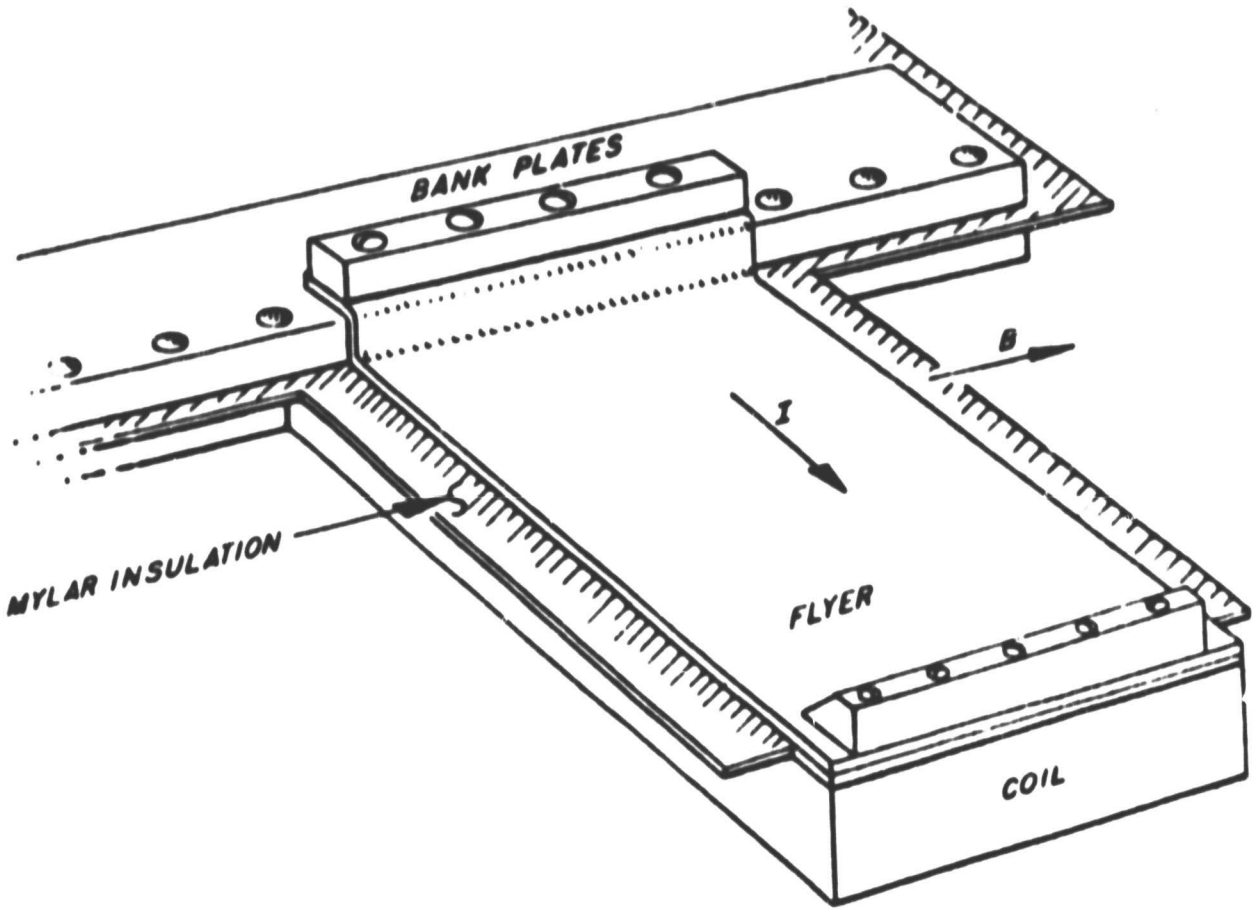

FIGURE 8. SCHEMATIC ILLUSTRATION OF A FLAT PLATE LOAD COIL ASSEMBLY.

SIMPLIFIED DESCRIPTION OF THE MAGNETIC FLYER TECHNIQUE

Physical Processes Involved

In the magnetic flyer technique for shock loading materials and structures, the stored energy of a capacitor bank is rapidly discharged into a single turn loop consisting of two series connected halves. As illustrated in Figure 9, one half of this single-turn loop consists of a massive back or load block into which has been machined a depression of geometry conforming to the shape of the structure to be impacted. Shapes of principal interest include frusta, hemispheres, and nosetips, the latter being a combination of a frustum and a hemisphere. Other shapes of interest include flat panels, rings, and cylinders. The second half of the single-turn loop is the flyer plate itself, formed from a thin metal sheet. The flyer plate typically is fashioned from aluminum sheet 5 to 33 mils in thickness. Composite metallic/non-metallic flyers are also employed. The significance of the flyer thickness and composition is that it controls the time duration and shape of the shock pressure pulse produced in the target material by impact of the flyer. The flyer, insulated from the load block by a thin layer of Mylar, is pressed into the load block depression. The structure to be impacted is placed into the depression a few millimeters in front of the flyer plate. The capacitor bank is then discharged into this single-turn loop. The equal but opposite megampere currents flowing in close proximity in the two halves magnetically accelerate the flyer in microseconds to a relatively constant supersonic velocity. By varying either the flyer-load block insulation thickness or

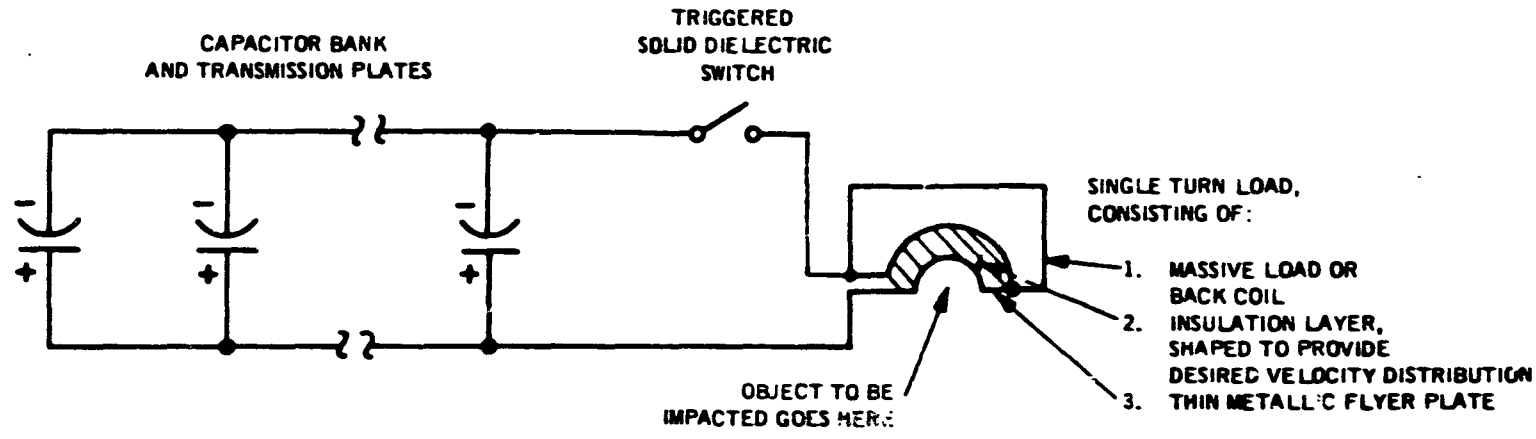

FIGURE 9. SCHEMATIC OF MAGNETICALLY DRIVEN FLYER PLATE SYSTEM.

the width of the flyer along the direction of the current flow (as illustrated in Figure 10), the flyer can be driven so that the velocity is the same from point to point upon the flyer or so that the velocity varies in a cosine or other distribution with respect to the flyer center line. By adjusting in addition the distance initially separating the flyer from the object to be impacted, one can attain simultaneity of impact over the entire planar or curved object surface. Under these conditions, the impact of the flyer upon the target results in the rapid deposition of a large amount of momentum and energy within a thin surface layer of the target material. Since this deposition occurs in a time which is short compared to a thermal conduction time, the material seeks to relieve itself of these locally high densities through the formation and propagation of a shock wave. This shock propagates through the material causing spallation and delamination at the rear surface. As the shock energy is attenuated during its propagation through the material, a portion of the shock momentum and energy goes into excitation of the structural normal vibrational modes and into rigid body translation.

These processes are illustrated in Fig. 11, which traces the flow of energy and momentum from the capacitor bank stored energy to the combined response, namely, the initial shock excitation in the material followed by excitation of the structural vibrational modes.

Quantitative Description

As indicated partially in Fig. 9, the system of capacitors, current transmission plates, load block and flyer constitute a series RLC circuit in which the switch is closed at t=0 resulting in a damped, oscillatory current flow. The differential equation for the current flow in a series RLC circuit I(t) has the form:

$$\frac{d}{dt}(LI) + IR + \frac{1}{c}\int I\ dt = V \qquad (1)$$

where V is the initial charging voltage of the capacitors and L and R denote the system inductance and resistance, respectively. Both the inductance

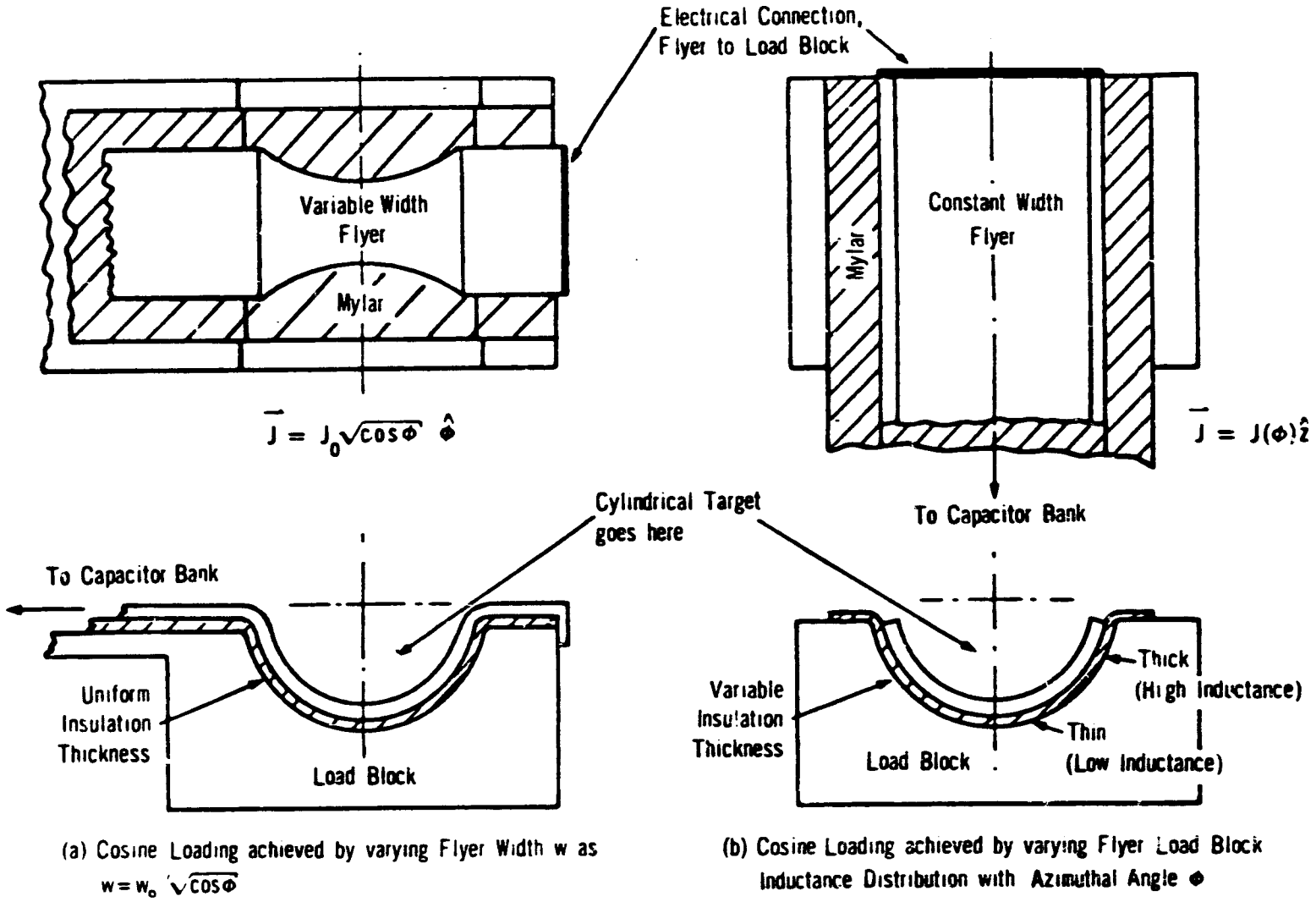

(a) Cosine Loading achieved by varying Flyer Width w as $w = w_o\sqrt{\cos\Phi}$

(b) Cosine Loading achieved by varying Flyer Load Block Inductance Distribution with Azimuthal Angle Φ

FIGURE 10. TECHNIQUES FOR DRIVING A FLYER TO A COSINE VELOCITY DISTRIBUTION.

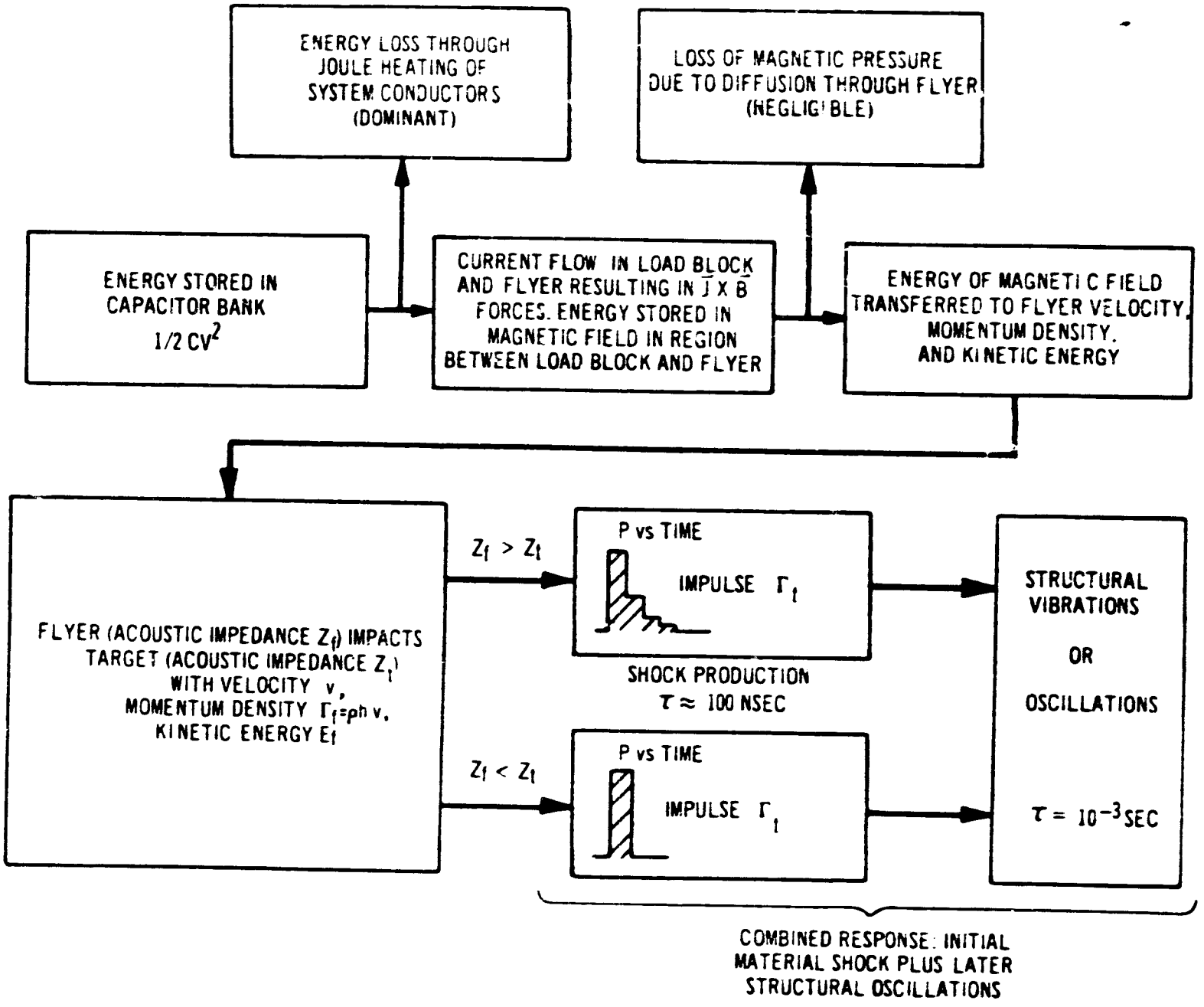

FIGURE 11. PHYSICAL PROCESSES INVOLVED IN MAGNETIC FLYER COMBINED RESPONSE IMPULSE TESTING.

and the resistance can be split into the sum of a constant part plus a time varying (increasing) part. The time-varying inductance component increases from zero at bank fire to a maximum value at target impact. This increase is due to the physical separation of the flyer from the load block. Similarly, the varying resistance component increases from zero to a maximum at impact. This term accounts for the transfer of system electrical and magnetic energy into the kinetic energy of flyer motion. Since each of these time-varying components form at most 10% of the total system resistance and inductance, we shall consider below solution of eqn (1) in which the time varying parts of L and R have been ignored. The results obtained agree with experiment to within 10% for most cases. The approximation breaks down as the product (target area) x (impulse) becomes large, or as 1) the flyer-block inductance at impact becomes comparable to the fixed system inductance and 2) the flyer kinetic energy at impact becomes comparable to the initial stored energy.

Quantitative Description

A quantitative description of the magnetically accelerated flyer technique should begin with the uniform velocity case, that is, the case of a flyer driven so that its velocity at any given time is the same from point-to-point. To this end, we shall consider the motion of a flyer of constant width w, mass density ρ , and thickness h through which flows a uniform current density $\vec{J}$ and total current I. The flyer is initially separated from the load block by an insulation layer of uniform thickness. This thickness (typically 10 to 40 mils) is small compared to both the flyer width and any flyer radii of curvature. The relative thickness of the flyer-load block insulation layer together with the series connection of the flyer and load block cause the current densities in the load block and in the flyer to have the same magnitude and distribution but opposite

flow directions. These equal and opposite currents result in the $\vec{J} \times \vec{B}$ acceleration of the flyer and lead to the result that the flyer velocity at any time is proportional to the time integral of the squared current.

As indicated earlier, the bank-flyer system is basically a series LRC circuit in which the switch is closed at t=0 thus connecting the charged capacitor to the system resistances and inductances. The values of the parameters R, L, and C are such that the system is underdamped, and the current flow is an exponentially damped, oscillatory function of time:

$$I = \frac{V}{\omega l} e^{-at} \sin \omega t \qquad (2)$$

where

V - bank charging potential

ω - system ringing frequency

L - system inductance

a - damping coefficient

C - system capacitance

R - system resistance

Expressions and values for some of these parameters are given below. These values are representative of a 350 kilojoule bank with aluminum conductors coupled to a load block-flyer system designed for a frustum 1 meter in length by 40 cm in base diameter. The values are presented in order to illustrate the orders-of-magnitude involved. They do not necessarily represent optimum values or the limits of the technique.

$$V \approx 55 \text{ kilovolts}$$

$$\omega = \sqrt{\frac{1}{C} - \frac{R^2}{4L^2}} \approx 8.8 \times 10^5 \text{ sec}^{-1}$$

$$L_o \approx 7\ n\ h$$

$$a = R/2L_o \approx 1.2 \times 10^5 \text{ sec}^{-1}$$

$$C = 182\ \mu\text{fd}$$

$$R \approx 1.7 \text{ milliohm}$$

$$\frac{a}{\omega} \approx 0.14$$

$$T = 2\pi/\omega = 7.1\ \mu\text{sec}$$

$$I_{max} = \frac{V}{\omega L_o} \exp\left(-\frac{\pi a}{2\omega}\right) \approx 7 \times 10^6 \text{ amperes}$$

Typically, upon switch closure, the flyer velocity increases from zero to a value several times the speed of sound in air in less than 3 or 4 μsec. It then travels another 3 or 4 μsec before simultaneously impacting the target. The total travel distance is 100 to 140 mils. For the times of interest, the flyer-to-load block distance is always small compared to both the flyer width w and any radii of curvature. Under these conditions, the $\vec{J} \times \vec{B}$ or magnetic forces accelerating the flyer may be modelled by the interaction between two parallel, planar current sheets of infinite extent. For such a system, the flyer magnetic force per unit area or pressure at any time is proportional to the squared current:

$$P = \frac{\mu_o}{2} \frac{I^2(t)}{w^2} \tag{3}$$

where μ_o is the permeability of free space (mks units). For this force density to be completely effective in accelerating the flyer, the flyer must have a sufficiently high conductivity σ and thickness h such that the lines of force do not diffuse through the flyer thickness for several microseconds. A time-independent criterion for this to occur and thus for the

validity of (3) is that the flyer thickness h be greater than the skin depth δ. The skin depth δ is defined by the expression

$$\delta = \sqrt{\frac{2}{\mu \sigma \omega}} = \sqrt{\frac{T}{\mu \sigma \pi}} = \sqrt{(2.53)(10^{-8})\, T/\sigma} \qquad \begin{array}{l}\text{in m for T}\\ \text{in } \mu\text{sec and } \sigma\\ \text{in units of } 10^7\\ (\text{ohm-m})^{-1}\end{array} \tag{4}$$

Listed below are the skin depths of several flyer materials for a 7 μsec bank ringing period.

Table 1. Skin depths for several materials, T = 7 μsec

Material	$\sigma(\text{ohm-m})^{-1}$	δ (mm)	δ (mil)	$\sqrt{\sigma_{mat}/\sigma_{Al}}$
Al	3.53×10^7	0.224	8.8	1.00
Cu	5.92×10^7	0.173	6.8	1.30
Ag	6.80×10^7	0.162	6.4	1.39

The square root ratio has been included as an index of improvement in going from aluminum conductors to some other material. We see that the 12 mil aluminum flyer in common use is about 1.5 skin depths thick. This seems to be satisfactory for the validity of (3) since as mentioned previously, the results derived therefrom are borne out by experiment to within about 10% percent.

The impulse per unit area Γ_u of the flyer as a function of time is given by the time integral of the pressure:

$$\Gamma_u = \int_0^t P(t')\, dt' = \frac{\mu_o}{4\pi} \frac{2\pi}{w^2} \int_0^t I^2(\tau)\, d\tau \tag{5}$$

This impulse delivered to the flyer by the magnetic field is manifested as flyer velocity or, more precisely, as the flyer momentum density $\rho h v$. It is flyer velocity which is usually measured to obtain Γ_f at impact. For an aluminum flyer of density $\rho = 2.70\ gm/cm^3$ and thickness h 12 mils = 0.305 mm, the relation between the flyer momentum per unit area Γ_f and the flyer velocity is

$$\Gamma_f = \rho h v = [(8.24)(10^3) v] \quad \begin{matrix} \text{in taps for v} \\ \text{in mm/}\mu\text{sec} \end{matrix} \qquad (6)$$

Through substitution of (2) into (5), we arrive at our major result, an expression for the flyer momentum density as a function of time:

$$\Gamma_u = \frac{\mu_o}{4\pi} \frac{2\pi}{w^2} \frac{\frac{1}{2} C V^2}{R} \left\{ 1 - e^{-2at} \left[1 + \frac{a^2}{\omega^2} (1 - \cos 2\omega t + \frac{\omega}{a} \sin 2\omega t) \right] \right\} \qquad (7)$$

Recall that this expression is valid for a flyer of constant width w accelerated to a uniform velocity or momentum distribution. The time factor in the curly brackets appears complicated, but in fact has simple properties if evaluated at fractional cycles and at $t=0$ and $t \to \infty$. The values are dependent only upon the ratio a/ω. In Table 2, the curly bracket is evaluated at several times for $a/\omega = 0.14$, a value representative of a large frustum system. Since we can arrange that impact occurs near $t = T \approx 7\ \mu sec$ for that system, we may ignore the curley bracket time factor and concentrate upon the remainder, which we define as Γ_u^∞:

$$\Gamma_u^\infty = \frac{\mu_o}{4\pi} \frac{2\pi}{w^2} \frac{\frac{1}{2} C V^2}{R} \quad \text{(uniform velocity case)} \qquad (8)$$

To go from ultimate impulse values to values at impact for the numerical values cited above, we assume impact $t = T$ and use the relation:

$$\Gamma_u \text{ (impact)} = \Gamma_u (T) = 0.83\, \Gamma_u^\infty \qquad (9)$$

Table 2. Curly bracket values for a magnetic flyer system.

Event	Value of ωt	Expression for $\{\ \}$	Value of $\{\ \}$ for $\frac{a}{\omega}$ 0.14
Switch closure	0	$\left\{ 0 \right\}$	0
quarter cycle of I(t)	$\frac{\pi}{2}$	$\left\{ 1-e^{-\pi \frac{a}{\omega}} \left(1 + 2 \frac{a^2}{\omega^2}\right) \right\}$	0.30
half cycle of I(t)	π	$\left\{ 1 - \exp\left(-2\pi \frac{a}{\omega}\right) \right\}$	0.58
full cycle of I(t) ($\approx$ impact time)	2π	$\left\{ 1 - \exp\left(-4\pi \frac{a}{\omega}\right) \right\}$	0.83
three half cycles of I(t)	3π	$\left\{ 1 - \exp\left(-6\pi \frac{a}{\omega}\right) \right\}$	0.93
infinity	∞	$\left\{ 1 \right\}$	1

The factor 0.83 in this specific example is just the curly bracket evaluated at $t = T$ for $a/\omega = 0.14$. It is important to note the dependence of Γ_u^{∞} upon the flyer width w, the bank energy $\frac{1}{2} CV^2$, and the system resistance R. The system inductance enters in a second-order fashion via the curly bracket time factor. Equation (8) for the uniform flyer case has the numerical expression:

$$\Gamma_u^{\infty} = \left[6.28 \times 10^4 \; \frac{\frac{1}{2} C V^2}{w^2 R} \right] \quad \begin{array}{l} \text{in taps for} \\ \frac{1}{2} C V^2 \text{ in KJ,} \\ R \text{ in milliohms,} \\ w^2 \text{ in cm}^2 \end{array} \qquad (10)$$

Recall that the tap is the conventionally used cgs unit of momentum density or impulse, i.e., 1 gm/cm-sec = 1 tap.

Described earlier and illustrated in Fig. 10 were two techniques for driving a flyer to a cosine velocity distribution. We seek expressions for the centerline or $\phi = 0$ flyer momentum density, analogous to those given in eqns. (7) and (8) for the uniform velocity case. Recall that both techniques involved a redistribution of the current density J to achieve acceleration forces which decreased monotonically from a maximum at $\phi = 0$.

In the first technique illustrated in Fig. 10 the flyer width depends upon azimuthal angle as

$$w = w_o \Big/ \sqrt{\cos \phi} \qquad (11)$$

Since the same total current I must flow through any flyer cross section of area wh, we can write the sequence

$$\begin{aligned} \text{const.} = I &= J(\phi) \cdot h \cdot w(\phi) \\ &= (J_o \sqrt{\cos \phi}) \cdot h \cdot \left(\frac{w_o}{\sqrt{\cos \phi}} \right) \\ &= J_o h w_o \end{aligned} \qquad (12)$$

where J_o and w_o are, respectively, the current density and flyer width at ϕ. Note that the current density varies only with ϕ and not with the coordinate z since the flyer-load block insulation is of uniform thickness. The reasoning embodied in eqn. (12) leads to the conclusion that the expression for the flyer centerline momentum density Γ_o has the same form as the uniform velocity case, but with the replacement $w \to w_o$:

$$\Gamma_o^{\infty} = \frac{\mu_o}{4\pi} \frac{2\pi}{w_o^2} \frac{\frac{1}{2} C V^2}{R} \quad \text{(cosine velocity case, resistive technique)}$$

$$= \left[6.28 \times 10^4 \frac{\frac{1}{2} C V^2}{w_o^2 R} \right] \quad \text{in taps for } \frac{1}{2} C V^2 \text{ in kJ, R in milliohms, } w^2 \text{ in cm}^2. \qquad (13)$$

Note that by varying the cross section or width of the flyer with azimuth, we are varying the resistance so as to achieve the current flow necessary for a cosine velocity distribution.

In the second technique, the flyer width remains constant. The current is re-distributed by varying the inductance as a function of azimuthal angle. This is accomplished by varying the flyer-load block insulation thickness so that it increases monotomically from a minimum at $\phi = 0$. To describe the effect of this current redistribution and obtain expressions for the centerline or $\phi = 0$ momentum density Γ_o for a flyer driven in this way to a cosine velocity distribution, we divide the uniform velocity expressions by the angular average $\langle \cos \phi \rangle$:

$$\Gamma_o^{\infty} = \frac{\mu_o}{4\pi} \frac{2\pi}{w^2} \frac{\frac{1}{2} C V^2}{\langle \cos \phi \rangle R} \quad \text{(cosine velocity case, inductance technique)}$$

$$= \left[8.91 \times 10^4 \frac{\frac{1}{2} C V^2}{w^2 R} \right] \quad \text{in taps for } \frac{1}{2} C V^2 \text{ in kJ, } w^2 \text{ in cm}^2, \text{ R in milliohns, } \langle \cos \phi \rangle = 0.705. \qquad (14)$$

The angular average $\langle \cos \phi \rangle$ is defined by the expression:

$$\langle \cos \phi \rangle = \frac{1}{2\phi} \int_{-\phi}^{+\phi} \cos \phi' \, d\phi' = \frac{\sin \phi}{\phi} \qquad (15)$$

The value of $\langle \cos \phi \rangle$ for ϕ 80^{o} is 0.705. Typically, cylindrically symmetric targets are loaded over the range $-80^{o} \leq \phi \leq 80^{o}$.

More detailed theoretical descriptions of the magnetic flyer acceleration process would include one or more of the following non-negligible physical effects:

1) non-uniformity of the current density across the width of a planar flyer, wherein the current increases sharply near the flyer edges from the relatively uniform interior current density;

2) the effect of joule heating in altering the flyer resistivity (an effect which may couple strongly with the enhanced edge currents to produce an inward-traveling peak of current density);

3) the effects of joule heating and the flyer thermodynamic state and phase (solid, liquid, and vapor when sufficient energy is available to drive the flyers to their ultimate momentum density);

4) the role of the relatively thin air layer between the flyer and the target from the point-of-view of its momentum and energy storage capabilities; and

5) the role of induced currents (and resultant fields) for conductive targets.

APPENDIX B

SHATTER/CONE EXPERIMENTAL MATRIX

January 21, 1980

Dr. Hal Linnerud
JAYCOR
300 Unicorn Park Drive
Woburn, MA 01801

Dr. Dave Roddy
U.S. Geological Survey
601 East Cedar Avenue
Flagstaff, Arizona 86001

Dear Hal and Dave:

This letter summarizes the meeting that Hal and I had on January 18 to plan a shatter/cone experimental matrix.

The purpose of the matrix is to systematically vary several of the parameters that have been postulated to play an important role in shatter cone formation. These parameters are:

(1) Heterogeneties in the rock
(2) Brittleness of the rock
(3) Stress amplitude
(4) Stress duration
(5) Flow conditions (planar vs divergent).

The level of effort does not allow an exhaustive parameter sensitivity study, so the enclosed preliminary test matrix does not examine soft or porous materials, but confines itself to relatively hard, non porous, brittle materials. The number of experiments will be between 10 and 20, depending on the number of materials actually used and the number of repetitions. The suggested materials are epoxy, rock-matching grout and/or (in response to our January 18 phone conversation, Dave) limestone. The epoxy (and perphaps the grout) samples will contain a size distribution of cast-in flaws. The flaws will all be significantly larger than the natural graininess of the material, but smaller than the input pulse width. Unflawed samples would also be tested as controls. Since the pulse widths producible in the proposed magnetic flyer laboratory experiments are on the order of a millimeter, the largest cast-in flaws must also be about a millimeter in size, with most of the flaws being on the order of 10-500 μm. They should be spaced about 1 mm apart, so their concentration should be about 10^{3} cm^{-3}. This should be feasible for epoxy at least, using glass microballoons for the flaws. The grout and limestone must be examined pre and post test carefully using petrographic techniques to get the flaw or grain size distribution.

The load parameters will be varied by using two different sized magnetic flyer plates, one large area flyer to produce uniaxial strain, planar flow over a significant region of the target, and one small area flyer to produce divergent flow. The divergent flow case can attain higher impact pressures, but is complicated by relief waves from the free portion of the impact surface. The impact pulse duration in the magnetic flyer experiments will be about 0.3 μsec and the corresponding pulse width in epoxy will be about 0.6 mm. Since most shatter cone theories state that the cones are formed in or near the shock front, any shatter cones formed would be expected to be of sub millimeter size, and must therefore be sought with the microscope in post test examination. Overall target sample dimensions of 10 cm x 10 cm x 10 cm will thus be sufficient to appear infinite.

In the epoxy experiments, high speed photography, in addition to pressure and particle velocity diagnostics, would be desirable. However, the small scale of the experiments suggests that the shatter cones would be formed in less than a microsecond, and this would exceed the space and time resolutions of normal framing cameras (as well as pushing that of stress and particle velocity gages).

A way out of this difficulty and, in addition, a way to extend the experiments to higher pressures, durations, and potential cone sizes, would be to detonate high explosive charges in the interiors of the specimens. By using a 1 cm charge diameter we could push the experimental scale sizes from millimeters to centimeters, thus making the potential cones more visible and the electronic and framing camera diagnostics more viable. Computer modeling of the spherical flow would also be easy Hal plans to approach George Ullrich at DNA to see if he would fund such experiments on a piggy back basis. These experiments are also listed in the matrix.

I personnaly would eventually like to see a fairly large scale epoxy shot with a charge diameter of several centimeters. This would make the framing camera completely feasible, and the stress and particle velocity gaging would also be easier. Finally, different internal flaw loadings could be put into different solid angles around the source, and we could get a lot of statistical information out of one shot. If we see shatter cones in the small scale experiments perhaps we can push for larger scale shots later.

In my view, it will be difficult to make shatter cones with the magnetic flyer experiments. In the planar impacts, the uniaxial strain flow

condition prevents tension from forming in the shock wave and limits the amount of elastic shear stress attainable to one fourth to three eighths the impact stress. This is why fracture is seldom seen in such experiments. The divergent flow case is more promising because the divergence can produce large hoop tensions and shear stresses. However, the relatively low impact stresses attainable will be quickly attenuated by relief waves from the edges of the impact. One approach considered by Hal and me to overcome this difficulty is to let the magnetic flyer transmit its pulse down a high modulus rod (ceramic or high strength steel) in a slightly larger diameter hole in the target. The transmitted wave at the bottom of the hole would then produce less attenuated divergent flow more like that from an internal explosive charge, albiet at a much lower amplitude and duration. Alternatively, if the whole rod were accelerated by a powder gun and impacted the bottom of the hole, the duration of the load would be governed by the rod length and could thus be varied. An inexpensive powder gun firing a steel rod at 1 km/s would produce 10-20 kbar in the target.

In summary, the action items are:

(1) Attempt to cast 50-500 μm diameter microballoons in 10 cm x 10 cm x 10 cm cubes of epoxy (and perhaps grout) with a uniformly dispersed concentration on the order of 10^3 cm^{-3}. (Grout cylinders are of course just as good as cubes. For epoxy, cubes are better optically.)

(2) Calibrate the SAI magnetic flyer facility and associated stress wave diagnostics.

(3) Arrange for fine-grained grout samples with and without cast-in microballoons to be made at Waterways Experimental Station, if possible.

(4) Obtain limestone samples.

(5) Think more about producing the divergent flow load with the magnetic flyer facility.

(6) Plan the post test methodology for looking for the shatter cones.

I plan to help out on item (5) above. Dave, you are clearly the best one to attack item (6); Hal and I are now waiting for your comments and suggestions. Hal's plan calls for testing to begin in March.

Best regards,

D. R. Curran
Department Director
Shock Physics and Geophysics
Poulter Laboratory

drc/im

Enclosure

Proposed Shatter Cone Experimental Matrix

	Load Parameters			Material Parameters	
	P_{max}(kbar)	τ(μs)	Flow	Material	Cast-in Flaw Sizes (μm)
Magnetic Flyer	50	0.3	Planar	Epoxy	0
	50	0.3	Planar	Epoxy	50-500
	50	0.3	Planar	Grout	0
	50	0.3	Planar	Grout	50-500
	50	0.3	Planar	Limestone	0
	100	0.3	Divergent	Epoxy	0
	100	0.3	Divergent	Epoxy	50-500
	100	0.3	Divergent	Grout	0
	100	0.3	Divergent	Grout	50-500
	100	0.3	Divergent	Limestone	0
High Explosive Charges	50	1.0	Divergent	Epoxy	0
	50	1.0	Divergent	Epoxy	50-5000
	50	1.0	Divergent	Grout	0
	50	1.0	Divergent	Grout	50-5000
	50	1.0	Divergent	Limestone	0
	150	1.0	Divergent	Epoxy	0
	150	1.0	Divergent	Epoxy	50-5000
	150	1.0	Divergent	Grout	0
	150	1.0	Divergent	Grout	50-5000
	150	1.0	Divergent	Limestone	0